UNIVERSIDAD DE CHILE
FACULTAD DE CIENCIAS FÍSICAS Y MATEMÁTICAS
DEPARTAMENTO DE INGENIERÍA INDUSTRIAL

MODELO ESTOCÁSTICO DE PLANIFICACIÓN FORESTAL : CONSECUENCIAS DEL CAMBIO CLIMÁTICO EN LA RED DE CAMINOS

TESIS PARA OPTAR AL GRADO DE MAGÍSTER EN GESTIÓN DE OPERACIONES
MEMORIA PARA OPTAR AL TÍTULO DE INGENIERO CIVIL INDUSTRIAL

IAN BORTNIC KREISBERGER

PROFESOR GUÍA:
ANDRÉS WEINTRAUB POHORILLE

MIEMBROS DE LA COMISIÓN:
RAFAEL EPSTEIN NUMHAUSER
JAIME CARRASCO BARRA

SANTIAGO DE CHILE
2020

RESUMEN DE LA MEMORIA PARA OPTAR AL
TÍTULO DE INGENIERO CIVIL INDUSTRIAL Y AL
GRADO DE MAGÍSTER EN GESTIÓN DE OPERACIONES
POR: IAN BORTNIC KREISBERGER
FECHA: 10/12/2020
PROF. GUÍA: ANDRÉS WEINTRAUB POHORILLE

MODELO ESTOCÁSTICO DE PLANIFICACIÓN FORESTAL : CONSECUENCIAS DEL CAMBIO CLIMÁTICO EN LA RED DE CAMINOS

El cambio climático tiene diversos impactos medioambientales, tales como el aumento de la temperatura terrestre, incendios y huracanes. En este trabajo, se estudian los cambios en la precipitación anual y el aumento de tormentas durante el siglo 21 en la localidad de Washington Sate, y cómo estos cambios se traducen en nuevos costos de reconstrucción de caminos. Así mismo, introducimos el primer modelo estocástico de adaptación óptima para la mantención de caminos y el acceso incierto a la materia prima, acompañado de un original conjunto de parámetros capaces to capturar el aumento en los costos de reconstructión, consecuencia de un aumento en la erosión terrestre y la destrucción de caminos provocado por tormentas de lluvia. Este modelo, llamado ARDM (Accelerated Road Decay Model), es aplicado en el área del rio Sol Duc, una zona forestal de 150 km^2 compuesta por una red vial de 63.5 km., ubicada en la zona norte del OESF (Olympic Experimental State Forest), Washington State. Mostramos además cómo este modelo aumenta el valor presente neto de esta zona al ser capaz de adaptarse a las precipitaciones a lo largo del siglo, evidenciando así los potenciales beneficios de incorporar esta nueva formulación en futuros modelos forestales de cosecha y reparación de caminos.

RESUMEN DE LA MEMORIA PARA OPTAR AL
TÍTULO DE INGENIERO CIVIL INDUSTRIAL Y AL
GRADO DE MAGÍSTER EN GESTIÓN DE OPERACIONES
POR: IAN BORTNIC KREISBERGER
FECHA: 10/12/2020
PROF. GUÍA: ANDRÉS WEINTRAUB POHORILLE

MODELO ESTOCÁSTICO DE PLANIFICACIÓN FORESTAL : CONSECUENCIAS DEL CAMBIO CLIMÁTICO EN LA RED DE CAMINOS

Climate change has serious environmental impacts, such as rising of global temperatures, fires and hurricanes. In this work, we study the changes in annual precipitations and more frequent storm events throughout the 21^{st} century in Washington State, and how they translate into new road reconstruction costs. We introduce the first stochastic formulation for optimal adaptation of forest roads maintenance and uncertain road access to timber resources, with a novel set of parameters that capture higher road reconstruction costs due to accelerated decay and even road failures caused by more intense storms. This model, called the ARDM (Accelerated Road Decay Model), is applied to the Sol Duc River drainage area, a 150 km^2 forest land base with a 63.5 km. road network infrastructure located in the northern part of the OESF (Olympic Experimental State Forest), Washington State. We show how this model increases the location's NPV by adapting its strategy to precipitation patterns along the planning horizon, thus showing the potential benefits of incorporating this formulation in future harvesting and road reconstruction schedules.

Acknowledgements

This thesis is the result of a collaborative work of an international team. I want to thank Andrés Weintraub, Sandor Tóth and Weikko Jaross for their contributions, guidance and constant support throughout this process.

Contents

1 Introduction **1**

2 Background **3**

3 The Endogenous Fixed Charge Model **6**

4 ARDM: Accelerated Road Decay Model **11**
4.1 The Effect of Higher Precipitation on Road Decay 11
4.2 The Effect of Extreme Storm Events on Road Failure 14
4.3 ARDM Cost Structure Summary 17

5 Data **18**
5.1 Climate Data 18
5.2 Forest and Road Data 23

6 Climate Data Processing and Scenario Generation **29**
6.1 Climate Data Processing 29
6.1.1 Extreme Event Probability Realizations 30
6.1.2 Extra Erosion Realizations 35
6.1.3 New Road Reconstruction Cost Realizations 38
6.2 Scenario Generation 40

7 Stochastic Program **42**
7.1 Scenario Tree: 42
7.2 Stochastic Program and Naïve Models 45

8 Results **47**
8.1 Deterministic Model 47
8.2 ARDM/Stochastic Model vs. Naïve Models 49
8.2.1 Schedule comparison: ARDM vs. NMs 55

9 Conclusions **59**
9.1 Final Thoughts 60

Appendix **61**
Bibliography 66

Chapter 1

Introduction

Forest planning has a rich research and development history of integrating timber harvest scheduling with forest road management. Efforts to integrate environmental impacts such as climate change are less common due to their inherent stochastic and uncertain nature and the computational complexity they present to mathematical programming. Climate change often results in more intense and more frequent precipitation events that can damage forest roads thereby compromising access to timber resources. Nonetheless, integrated forest harvest scheduling models allow forest managers to jointly optimize the spatiotemporal allocation of silvicultural actions, such as harvests, as well as road construction and maintenance decisions across the landscape and over time to mitigate these negative effects.

In the past decades, forest harvest scheduling problems were typically formulated as deterministic optimization models. Deterministic models are not ideal when the values of some key parameters, such as forest growth and yield are uncertain due to climate change. Climate change is expected to lead to a more vigorous hydrological cycle (Nearing et al., 2004), both in terms of global air temperatures and precipitation patterns coupled with increased risk of fire, windstorms and landslides. Changes in the intensity, duration, and frequency of precipitation will negatively affect forest roads - already the biggest financial and environmental liability in timber management. Damaged roads can increase sediment delivery (Bowker et al., 2010; Bettinger et al., 1998; Riedel & Vose, 2003) to streams and thus compromise fish habitat. Reduced access can also make wildfire detection and control more difficult to implement. With climate change, roads will be vulnerable to higher annual precipitation and more intense storms, leading to higher runoff and soil erosion rates. More frequent and severe storms may also cause major changes in hydrology and channel morphology, making current culverts[1] unable to accommodate future channel conditions, which will in turn create barriers to fish movement (Wilhere et al., 2017).

Neglecting these changes can lead to sub-optimal harvest schedules and reduce timely access to harvest units. In the absence of preemptive measures, maintenance costs would rise due to higher road surface erosion rates and more pressure on bridges and culverts. Nonetheless, financial losses can be mitigated by adapting the maintenance and reconstruc-

[1]Culvert: A tunnel carrying a stream or open drain under a road or railway.

tion schedule of forest road networks to projected increases in the frequency and intensity of extreme but uncertain weather events (Chinowsky and Arndt (2012)). This can be done in several ways. By anticipating road damages and reduced access to timber as a result, managers could opt to accelerate harvesting in vulnerable areas before these assets are lost. They could also choose to upgrade roads, culverts and bridges to higher standards sooner, thereby preempting structural failures due to increased storm intensities. Lastly, they could also time harvests strategically so that only a small subset of vulnerable road segments would have to be used for hauling.

Stochastic programming models have been proposed in the past for forest planning in the face of volatile timber prices, demand uncertainty (Veliz et al., 2015) and climate change. Prior work on climate change uncertainty mostly focused on changes to growth and yield (Quinteros et al., 2011). Little has been done in the way of addressing the effects of storms on road access, transportation and costs. This is a problem because forest roads are very expensive and at the same time are likely to constrain the spatiotemporal viability of harvest plans (Ross et al., 2018). Our proposed model is the first formulation for optimal adaptation of forest roads maintenance and uncertain road access to timber resources due to climate change. We created a stochastic formulation of the integrated harvesting problem with a novel set of parameters that capture higher road reconstruction costs due to accelerated decay and even road failures caused by more intense storms. In addition, our model can be applied beyond forestry. For example, transportation problems in mining, trucking, railroads and logistics in general present similar risk profiles as damages to and losses of structures in these industries also occur in a probabilistic manner.

To illustrate our model, we built 27 road cost scenarios to represent accelerated decay and storm probabilities using 12 regional climate models. The regional climate models were used to project hourly precipitation rates from 2010 until 2100 across a 150 km^2 forested landbase in the Pacific Northwest United States. We assumed that road reconstruction costs will increase with accelerated decay due to higher annual precipitation and increasing probabilities of extreme storm events. To show the benefits of incorporating climate projection data in harvest schedules, we constructed a stochastic model and compared it to 4 naïve models used as benchmarks to represent standard industry practices. One of these models does not consider climate change at all, and the 3 other that do do so but in a deterministic fashion. We show the financial benefits of our model's ability to adapt road reconstruction decisions to future climate scenarios, and also analyze the differences in the harvest and reconstruction schedules between the stochastic and naïve approaches.

Chapter 2

Background

The goal of forest management is to achieve strategic objectives such as sustainable timber supply over large land areas and long planning horizons subject to a variety of environmental, economic and logistical constraints. The strategic directions that guide forest management over the long term are generated by strategic harvest scheduling models.

Forest planners can adjust harvest schedules to changing circumstances by periodically re-assessing current conditions against strategic directions, then re-allocating limited capital to the right place at the right time. They are responsible for selecting appropriate, site-specific forest practices, to accomplish desired economic performance, forest health, watershed, and wildlife habitat objectives, including a diversity of tree species and age classes.

Forest planning models have evolved over the decades to generate more efficient harvest schedules at lower costs. With increasing computing power, analysts have incorporated an increasing amount of complexity in these mathematical models. Prior to the 1970s however, road construction decisions were made only after the harvest schedules were finalized. This lead to inefficiencies in the form of temporal misalignments between harvest timings and road (re)construction schedules (Johnson & Scheurman, 1977). Weintraub and Navon (1976) were one of the earliest authors to develop a mixed-integer programming model (MIP) to integrate these two sets of critical forest management decisions in a single formulation. This was followed by Kirby et al. (1980) "Integrated Resource Planning Model", which illustrated the benefits of this integration. In 2003, Andalaft et al. developed a mixed-integer LP model to solve complex instances of the integrated harvesting problem, and successfully implemented it in a real Chilean forestry firm. By strengthening the model formulation using efficient trigger constraints and lifting techniques coupled with a Lagrangean relaxation method, the authors were able to create a model that gave good solutions in a reasonable computing time (something that commercial codes were unable to do during that time).

Another breakthrough occurred when Ross et al. (2018) found a way to model road maintenance costs as an endogenous function of harvest scheduling decisions. The authors applied their model, the "Endogenous Fixed Charge Model" (EFCM), to the the Upper Clearwater River Landscape (UCRL) on the Olympic Peninsula of the Pacific Northwest United Sates. This case study forest comprised 621 operable Forest Management Units (FMUs) and over

6,000 road segments. The EFCM was able to improve the valuation of the UCRL by 0.5 - 1 million USD and reduce the length of the active road network by 14.5%. A win-win achievement.

Apart from deterministic harvest models, stochastic formulations have also been developed in order to account for uncertain parameters that materialize over long planning horizons (Quinteros et al., 2011; Veliz et al., 2015; Sanei Bajgiran et al., 2017; Alonso-Ayuso et al., 2018)) . For example, Alonso-Ayuso et al. constructed an MIP multi-period stochastic harvest and road building model that accounts for uncertain timber prices and demand over time. They were able to show the benefits of using a stochastic model for a risk averse decision maker in the forest industry, and demonstrated that these models shift profitable activities to earlier planning periods at a relatively small loss of profit at the end of the planning horizon.

On the other hand, with climate models predicting major changes in precipitation and air temperature patterns, several analysts have started to incorporate uncertain climate impacts on long-term timber supply. In 2007, Garcia-Gonzalo created a model to incorporate the effects of increasing temperatures, precipitation, and atmospheric CO_2 on forest level carbon stocks in Finland and timber production management. The author observed between 3.4% and +9.2% increase in valuation, 30% to 50% of which was attributable to the optimization model while the rest of the gains came from increased production due to climate change. Later in 2009, Latta et al. (2009) developed a simultaneous autoregressive (SAR) model to estimate the impacts of climate change on potential productivity of Pacific Northwest (PNW) forests in the United States. They found considerable variation in potential productivity change across both time and space within the region. They were also able to pair climate data with emission concentration pathways provided by the IPCC to identify regions more susceptible to climatic change under different future scenarios.

Another approach at incorporating climate change in timber supply analysis was done by Diaz et al. (2015). By using a Forest Vegetation Simulator (Climate-FVS), their model predicted negative impacts attributed to climate change, such as declining growth and yield projections, large-scale shifts in forest composition and increases in tree mortality and fire hazards. The author showed that a disregard for climate change impacts on future growth-and-yield and its potential severity is likely to produce unrealistic models and inadequate harvesting schedules for the future.

Apart from future timber supply analysis, researchers have studied how road infrastructure is going to be affected by climate change. Regional climate models predict increasingly severe and frequent natural disturbances such as floods and landslides. This suggests that forest infrastructures are going to be at greater risks of decay and loss. While there are many examples of climate impact assessments for road infrastructure in western Washington and Oregon (Halofsky et al. (2011); Raymond et al. (2014), among others), the methodologies have generally focused on the mapping and ranking of hazards to roads such as inundation and flooding, stream bank erosion, and increased slope failures.

Analysts argue that while climate change poses costly impacts on road networks in terms of maintenance, repairs and lost connectivity, many of these impacts can be mitigated or even avoided by appropriate adaptation measures. Chinowsky and Arndt (2012), for example,

developed an analytical framework known as the Infrastructure Planning Support System (IPSS) to automate the computational burden of a climate based scenario analysis. This tool uses an engineering and materials based stressor-response functions to determine the impact of climate on maintenance, repair and road construction to provide a longer-term approach to the management and planning of road infrastructure.

Although much work has been done on analyzing how climate change will affect forest harvest scheduling, in the present thesis we introduce the first stochastic integrated harvest and road (re)construction scheduling model that incorporates the effects of climate change on access to timber resources. We build on the EFCM and construct a *pro-active adaptation* strategy that incorporates stochastic road reconstruction parameters due to accelerated road erosion rates as a consequence of increasing annual precipitation, and also due to rare but devastating storm events fueled by climate change. Our proactive adaptation strategy involves changes in the spatiotemporal allocation of road maintenance activities as well as road upgrades in an attempt to increase system resilience to various climate stressors. As it was previously pointed out, our model can be applied beyond forestry in many other industries facing potential adverse effect to their transportation network.

We start with a formal mathematical description of the EFCM, as well as its underlying assumptions, before introducing the new stochastic elements that concern road access.

Chapter 3

The Endogenous Fixed Charge Model

The Endogenous Fixed Charge Model, or EFCM, is a mixed integer program (MIP) developed by Ross et al. (2018), whose objective function maximizes net present value (NPV): discounted timber revenues minus discounted costs, such as harvesting, road maintenance and reconstruction costs. The term *endogenous* comes from the fact that reconstruction costs not only depend on external factors such as weather but also on prior road reconstruction and maintenance actions whose timing is to be optimized by the model itself.

The EFCM is built on the Johnson and Scheurman (1977) Model II formulation with the use of added variables and constraints that represent road maintenance decisions and associated costs. Model II itself is a linear program (LP) that optimizes how much of each FMU (forest management unit) should be harvested in a given planning period to maximize NPV. The model is subject to a variety of constraints such as sustainability requirements, even harvest volume flows, ending horizon conditions and other ecological considerations. Formally, it can be described as follows:

Model II Formulation

Given the following model parameters and set notation,

$$
\begin{aligned}
M &= \text{the set of all FMUs,} \\
P &= \text{the oldest age class in the initial inventory,} \\
Z &= \text{minimum rotation age in decades,} \\
A_m &= \text{the area of FMU } m \text{ in hectares,} \\
a_{m,t} &= \text{percent of FMU } m \text{ that is in age class } t \text{ in period 1,} \\
v_{m,t_1,t_2} &= \text{volume/ha in FMU } m \text{ for harvests of age class } t_2\text{-}t_1, \\
\rho_{m,t_1,t_2} &= \text{revenue/ha in FMU } m \text{ for harvests of age class } t_2\text{-}t_1, \\
Age_{t,l} &= \text{age of an FMU regenerated in } t, \text{ in period } l. \text{ e.g. } Age_{2,9}=7,
\end{aligned}
$$

and decision variables,

$$W_{m,t_1,t_2} = \% \text{ of FMU } m \text{ regenerated in } t_1 \text{ and harvested in } t_2,$$
$$N_{m,t} = \% \text{ of FMU } m \text{ regenerated in } t \text{ that will never be harvested,}$$

Model II can be stated as:

$$\max \quad \sum_{l=1}^{|T|} \sum_{k=-P}^{l-Z} \sum_{m} A_m \rho_{m,k,l} W_{m,k,l}, \tag{3.1a}$$

$$\text{s.t.} \quad N_{m,k} + \sum_{l=1}^{|T|} W_{m,k,l} = a_{m,k}, \qquad \forall m \in M, k = -P, ..., 0, \tag{3.1b}$$

$$N_{m,k} + \sum_{l=k+Z}^{|T|} W_{m,k,l} = \sum_{t=-P}^{k-Z} W_{m,t,k}, \qquad \forall m \in M, k = 1, ..., |T|, \tag{3.1c}$$

$$\sum_{m} \sum_{k=-P}^{l-Z} v_{m,k,l} W_{m,k,l} = H_l, \qquad \forall l = 1, ..., |T|, \tag{3.1d}$$

$$1.25 H_t \geq H_{t+1} \qquad \forall t = 1, ..., |T| - 1, \tag{3.1e}$$

$$0.75 H_t \leq H_{t+1} \qquad \forall t = 1, ..., |T| - 1, \tag{3.1f}$$

$$\sum_{m} \sum_{t=-P}^{|T|} Age_{t,|T|} N_{m,t} A_m \geq \sum_{m} \sum_{t=-P}^{-1} Age_{t,1} a_{m,t} A_m \tag{3.1g}$$

Objective function (3.1a) maximizes NPV across all FMUs and planning periods. Logical constraints (3.1b) state that the sum of acres in FMU m that are in age class k in period 1 must be equal to the sum of acres that are assigned to be cut in a future planning period, plus those that are assigned not to be cut from FMU m during the complete planning horizon. Constraint set (3.1c) represents the flow of harvests considering the minimum rotation age Z. These constraints state that starting from period $k \geq 1$, the total area harvested and regenerated in FMU m in period k will either not be harvested again for the rest of the planning horizon, or will be harvested in some periods in the future (Z periods after period k). Equality (3.1d) is an accounting constraint that calculates the sum of all harvest volumes for each period. Inequalities (3.1e) and (3.1f) are even flow constraints that limit the difference in harvest volumes between consecutive planning periods to be no more than 25%. Finally, constraint (3.1g) is a minimum average ending constraint. It requires that the area-weighted average age of all FMUs at the end of the planning horizon is greater than at the start.

Using Model II as its foundation, the EFCM introduces binary variables to represent road reconstructions decisions, along with corresponding coefficients that show the associated costs of those decisions. The EFCM assumes that road segments must be upgraded to local or regional standards before they can be used for hauling. This means that if road segment i

will be used in period t, then a full road reconstruction has to be done on that segment at the beginning of period t for it to meet the standard conditions for hauling. The EFCM also assumes road segments degrade over time based on a user-defined schedule, which means that road reconstruction costs increase with the number of years that have elapsed without repair. This is the reason for the use of the word *endogenous* in EFCM. Fixed maintenance costs increase with time in disuse, which in turn is a function of the harvest schedule itself. In particular, if the number of years that have gone by since a road segment's last reconstruction exceeds a threshold, then a full repair is necessary, at full reconstruction cost. In contrast, repairing the road earlier than the threshold allows reconstruction at less than the full cost. The exact function for road decay can be adjusted as needed to approximate any decay pattern. For example, if we assume that a road segment i degrades in t_{max} years, and t years have already gone by since the last reconstruction, then its *Reconstruction Cost* is the following[1]:

$$Reconstruction\ Cost = Full\ Cost * \min(1, \frac{t}{t_{max}}).$$

EFCM Formulation

Given the following set notation,

M = the set of all FMUs,
I = the set of all road segments,
J = the set of cost tiers. For our work, $|J| = 2$,
T = the set of 10 year planning periods, indexed by $t = 1, 2, ..., |T|$,
V = the set of all vertices in the road network,
E = the set of edges (roads), defined by starting and ending vertices (p, q),
q_{out} = the set of vertices that can be reached from vertex q (outflow),
q_{in} = the set of vertices that lead to vertex q (inflow),
U_q = the set of FMUs that use vertex q as an entry point to the network,
V_τ = the set of vertices that are considered exit points for the network, and
τ = the "imaginary" sink vertex to which all vertices in V_τ are connected.

and parameters:

$\rho_{m,t}$ = net discounted timber revenue associated with harvesting FMU m in period t,
ϕ^j = fraction of full reconstruction cost for segment last reconstructed j periods earlier,
α_i = the total reconstruction cost of road segment i, and
N = an Arbitrary large number, greater than the maximum possible flow.

[1]Non-linear decay functions can also be incorporated in the EFCM formulation

and variables:

$x_{m,t} = 1$ if FMU m is harvested in period t, 0 otherwise,

$s^j_{i,t} = 1$ if road segment i is to be reconstructed in period t at cost $\phi_j \alpha_i$, 0 otherwise, and

$F_{(p,q),t} =$ the flow between vertices p and q in period t.

the EFCM can be stated as:

$$\max \quad \sum_{m,t} \rho_{m,t} x_{m,t} - \sum_{i,j,t} \phi_j \alpha_i s^j_{i,t} 1.05^{10(1-t)} \tag{3.2a}$$

$$\text{s.t.} \quad \sum_{j} s^j_{i,t} \leq 1 \qquad \forall i \in I, t \in T, \tag{3.2b}$$

$$\sum_{k=1}^{J} s^k_{i,t-j} \geq s^j_{i,t} \qquad \forall i \in I, t \in T, j \in J, \tag{3.2c}$$

$$\sum_{p \in q_{in}} F_{(p,q)} + \sum_{m \in U_q} x_{m,t} = \sum_{k \in q_{out}} F_{(q,k),t} \qquad \forall q \in V, t \in T, \tag{3.2d}$$

$$\sum_{p \in V_\tau} F_{(i,\tau),t} = \sum_{m} x_{m,t} \qquad \forall t \in T, \tag{3.2e}$$

$$N \sum_{k} s^k_{(p,q),t} \geq F_{(p,q),t \in T} \qquad \forall (p, q \neq \tau), t \in T, \tag{3.2f}$$

$$x_{m,t} \in \{0,1\} \qquad \forall m \in M, t \in T, \tag{3.2g}$$

$$s^j_{i,t} \in \{0,1\} \qquad \forall i \in I, t \in T, j \in J \tag{3.2h}$$

Objective function (3.2a) maximizes NPV: discounted harvest revenues minus the discounted road reconstruction costs. We assume that harvests and road reconstructions occur at the start of each period and applied a discount factor accordingly (this is a common practice in harvesting models). Constraint (3.2b) ensures that road segments can only be reconstructed at one cost tier. This is done by allowing the activation of only one of the following variables at any given planning period: $s^1_{i,t}, s^2_{i,t}, ..., s^{|J|}_{i,t}$. If none of these variables are activated in period t, it means than there was no reconstruction done and therefore hauling is not allowed through segment i (it does not meet the local standards). Constraint (3.2c) represents the tiered structure of endogenous road reconstruction costs. It says that road segment i can only be reconstructed at cost tier j in period t, if $s^k_{i,t-j} = 1$ for one value of k. In other words, the segment was reconstructed at any particular cost exactly j planning periods ago.

An important aspect of the EFCM is that it finds optimal hauling routes dynamically to support harvest actions. To achieve this, the road network is modeled as a directed graph, where edges represent road segments that carry flow and vertices represent intersections that connect the segments. Constraint (3.2d) ensures preservation of flow through the network. It makes sure that everything that flows into vertex q, including flows that originate in q

as a source, must be equal to the total amount of flow leaving vertex q. Using "imaginary" vertex τ as a sink, constraint (3.2e) ensures that the total flow that is produced across all the FMUs exits the system. To connect the flow constraint with the road reconstruction variables, inequality (3.2f) ensures that no flow is allowed to go through edge (p,q) in period t if the corresponding road segment is not reconstructed in that period. Parameter N allows even the maximum flow to pass through this edge if it is available for hauling.

In order to connect the EFCM's binary road reconstruction variables to Model II's continuous harvest decisions, the following pair of trigger constraints are added:

$$\sum_{k=-M}^{t-Z} W_{m,k,t} \geq H_{min} x_{m,t}, \qquad \forall m, t, \tag{3.3}$$

$$\sum_{k=-M}^{t-Z} W_{m,k,t} \leq H_{max} x_{m,t}, \qquad \forall m, t. \tag{3.4}$$

Constraint (3.3) allows the binary harvest indicators $x_{m,t}$ of the EFCM to switch on when a threshold percent (H_{min}) of a FMU's area is scheduled for harvest per Model II in period t. If no harvest is scheduled to occur in an FMU in period t, constraint (3.3) forces the harvest indicator to be zero. Working together with constraint (3.3), constraint (3.4) forces $x_{m,t}$ to be equal to 1 if the area to be cut from the FMU is greater than 0, with a maximum allowable value of H_{max}. Finally, the objective function of the joint model will be the same as in Model II (1a) minus the road reconstruction costs from (3.2a) in the EFCM. The integrated model is listed in Appendix A.)

Chapter 4

ARDM: Accelerated Road Decay Model

In this work, we present a novel climate adaptation model for forest road networks that face accelerated decay due to climate change. This model, which we will call the *Accelerated Road Decay Model*, or ARDM, is an extension of EFCM. Our proposed spatio-temporal model is the first to optimize climate adaptation in integrated natural resource and support infrastructure management. Two effects of climate change were analyzed: accelerated road decay due to higher precipitation, and road failure due to extreme rainfall events.

4.1 The Effect of Higher Precipitation on Road Decay

In the EFCM, decay functions of any form, linear or otherwise, can be incorporated by changing the values of vector ϕ. When the EFCM was applied to the Upper ClearWater planning area, the road segments were assumed to degrade linearly over a fixed 30-year period regardless of their location within the watershed or any other external factor (temperature, precipitation, etc.). This meant that a road not used for timber haul for 30 years or more required full reconstruction, whereas a road that was last reconstructed 20 years ago needed a reconstruction that cost one third less, and one reconstructed within the past 10–20 years cost two thirds less. This meant that the total number of cost tiers J was set to 3, $\phi^3 = 1$, $\phi^2 = \frac{2}{3}$ and $\phi^1 = \frac{1}{3}$ ($\phi^j = \frac{j}{3}$). In the present model, roads are no longer assumed to degrade linearly, but instead, their decay is going to be a function of future climate conditions. If future erosion rates are projected to be different from what they are today due to climate change, the generalized cost function that we propose can easily be adjusted to accommodate accelerated or decelerated decay schedules. This assumes that soil erosion [1] (Fig. 4.1a) and surface runoff [2] (Fig. 4.1b) are the primary drivers behind forest road decay, which in turn are directly correlated with annual precipitation rates due to rainfall erosivity [3].

[1]Erosion: Action of surface processes, such as water flow or wind, that removes soil, rock, or dissolved material from one location and then transports it to another location.

[2]Surface runoff: Flow of water that occurs when excess storm-water, melt-water, or other sources flow over the surface. This can occur when the soil is fully saturated and rain arrives more quickly than soil can absorb it.

[3]Rainfall erosivity: The ability of rain to cause soil loss as a result of the kinetic energy in raindrops striking the soil.

Using different combinations of soil types, slope gradients, and locations across the United States, Pruski and Nearing (2002) conducted a study to asses the relative influence of changes in annual precipitation on runoff and erosion. They showed that for every 1% increase in annual precipitation, we can expect a 2% and 1.7% increase in annual runoff and erosion, respectively. For this work, future erosion rates for every climate scenario were calculated using this idea. If future projections predicted an $x\%$ higher precipitation for the next 2 decades, then the extra erosion was set to $y\% = 2{*}x\%$ higher (runoff and erosion were modeled as on single effect generalized as "erosion", and the consequent value for every 1% increase in annual precipitation was set to an equivalent 2% higher annual erosion rate).

(a) (b)

Figure 4.1: Surface Erosion (a) and Surface Runoff (b)

When the EFCM was applied in the Upper ClearWater landscape on the other hand, the Washington State Department of Natural Resources (DNR) assumed that roads degrade linearly in a fixed 30 year period. Apart from the accelerated decay effect due to higher precipitations, in our study we assume that roads depreciate over 20 years. This assumption reduces the number of variables (2 cost tier reconstruction decisions instead of 3) and complexity of the problem, which we found was necessary to get the computational results needed for the stochastic program (this will be explained with more detail in the **Results Section**).

The fixed time decay idea is partially based on the assumption that there is not going to be a significant climate change in the next decades. But, if precipitation intensity does increase in the future, roads will get in worse conditions earlier in the decade. Land owners, who are responsible of building road segments able to withstand future climate conditions, will have to build stronger and more expensive road structures capable of holding for the full 20 years.

The next example shows how accelerated decay due to higher precipitations was incorporated in the ARDM's cost structure: Let's suppose that in a free-climate change scenario, road segment *i's* lifecycle is 20 years, and has a full reconstruction cost of C_i (this cost is proportional to the length of the road segment). This means that the DM can reconstruct road segment i at cost C_i and be sure it will last 20 years before needing a new full reconstruction. Now, in a climate change scenario, with more frequent and intense annual precipitations, the speed at which road *i's* degrades will increase and its lifespan will be reduced. If the extra

erosion in the next 20 years is $y\%$ higher, then the new lifecycle of road segment i can be calculated as *New Life Cycle*$_i$= $\frac{20}{1+\frac{y}{100}}$, where we are assuming that an extra erosion of $y\%$ translates into an $y\%$ faster decay. For example, if y=15, then the new lifecycle of road segment i is 17.4 years.

Now, it is required by law that when reconstructed, roads have to be upgraded to standard-/local conditions. In the context of our work, standard conditions mean that road segments will be able to hold for 20 years before exceeding the time threshold in disuse at which roads require full reconstruction before being used again for hauling. However, in the presence of climate change and more extreme weather scenarios, roads will have shorter lifespans (less than 20 years) if they are built with the usual infrastructure. On the other hand, a forester could anticipate faster erosion and build a stronger architecture at a higher cost, compensating the extra erosion with a tougher infrastructure. Continuing with the previous example, where the extra erosion over road segment i is 15% and consequently has an expected lifespan of 17.4 years (instead of 20), the forester could apply a preemptive measure by anticipating tougher weather, and decide to pay $\hat{C}_i = C_i \cdot \frac{20}{17.4} = 1.15 * C_i$ for road segment's i reconstruction, instead of C_i, and guarantee a lifespan of 20 years instead of 17.4 (assuming that the forester made a good prediction and the extra erosion in the next 20 years was indeed 15%).

In conclusion, if a particular road segment i is *expected* to experience an extra erosion of $y\%$ over the next 20 years, then the new standard full reconstruction cost is:

$$\hat{C}_i = C_i \cdot (1 + \frac{y}{100}) \tag{4.1}$$

By paying $\hat{C}_i$, and if the $y\%$ extra erosion for the next 20 years holds, then the DM can be certain that the new stronger infrastructure will compensate the extra erosion and ensure a lifespan of 20 years before requiring a new full reconstruction.

However, because future climate intensity is unknown and its consequences only reveal themselves with time, we cannot talk about one true deterministic $\hat{C}_i$ that ensures an exact 20 year lifespan for road link i: this value depends on an unknown extra erosion parameter y. The problem is that the DM can underestimate the y value and build a frail road infrastructure that is not able to withstand the next 20 years of higher future erosion rates. If this is the case, and for some particular period the DM does not observe the intensity he/she was expecting and prepared for, he/she acknowledges it and the state charges an extra maintenance fee as a tax for the higher maintenance costs needed to sustain the road link during the standard 20 years. On the other hand, if the DM overestimates the effects of future climate change and builds an unnecessary robust infrastructure, the state will refund the forester with the extra money invested. This is done by assessing the DM's schedule and adjusting the OF downward in scenarios where the reconstruction was done with a lower quality than what was needed. In the second case, where the road was constructed at a unnecessary high standard, the state adjust the DM's OF upward, giving him/her an extra fee for the extra expenses.

4.2 The Effect of Extreme Storm Events on Road Failure

In addition to changes in annual precipitation, climate models forecast major increases in storm intensities and frequency across Washington State over the 21^{st} century (Salathé Jr et al., 2014; Warner et al., 2015). These changes have major consequences on tree growth and yield, but they also on road segments and their reconstruction cost structure. Higher precipitation rates can cause landslides, higher soil erosion and runoff rates (Pruski & Nearing, 2002), increase soil particles spilling to rivers and create more extreme river flow patterns (Elsner et al., 2010).

In the Pacific Northwest, two factors interact to cause increases in flood magnitudes: decreasing precipitation stored as snow and intensifying heavy rain events (Pruski & Nearing, 2002). The predicted changes in stream flow across the PNW will cause alterations in channel morphology because they adapt their geometry to accommodate changes in discharge (Leopold & Maddock, 1953). This may have serious environmental consequences, one of them being the malfunctioning of culverts, as it is explained in (Fig. 4.2):

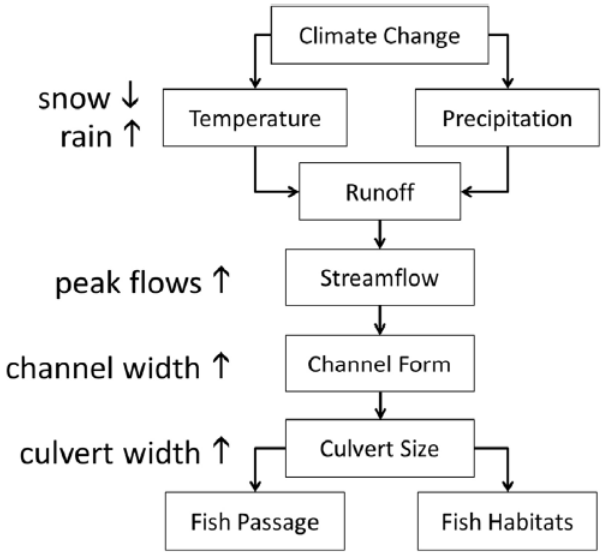

Figure 4.2: Causal relationships between culvert alteration and climate change. Climate change is projected to increase the proportion of precipitation that falls as rain rather than as snow. As a result, winter peak flows in most of Washington are expected to increase in volume. Increased peak flows are known to alter channel morphology. Wider channels require wider culverts, which if not replaced, can affect fish passage through the culvert and also nearby fish habitats (Wilhere et al., 2017).

Properly built culverts at river road crossings allow the correct passage of water and fish. They are designed to maintain the continuity of channel structure and composition by conveying water, sediment, and wood in the same way as the surrounding stream reach (Gillespie et al., 2014), and so fish are able to migrate through an artificial channel that closely simulates the key channel characteristics:

Figure 4.3: Culvert: A tunnel carrying a stream or open drain under a road or railway. They are designed to preserve the channel structure allowing water and fish passage.

One of the most important parameters of culvert design is bank-full width (a channel's width at its bank full elevation (Fig. 4.4)), and this is expected to increase in many parts of Washington State due to climate change (Wilhere et al., 2017). If this changes are not internalized in culvert management by repairing or replacing them, then fish passage will be seriously compromised because of sediment barriers and dangerous flow velocities through culverts. This is a critical issue in Washington State because several salmonid species are listed as threatened with extinction under the federal endangered Species act, which may get worse if the blockades at culverts issue is not properly addressed. This is also a legal problem because in 2013 a federal court ruling determined that the United States government had to grant Native American tribes the right of a protected fish habitat (United States vs. Washington (2013)).

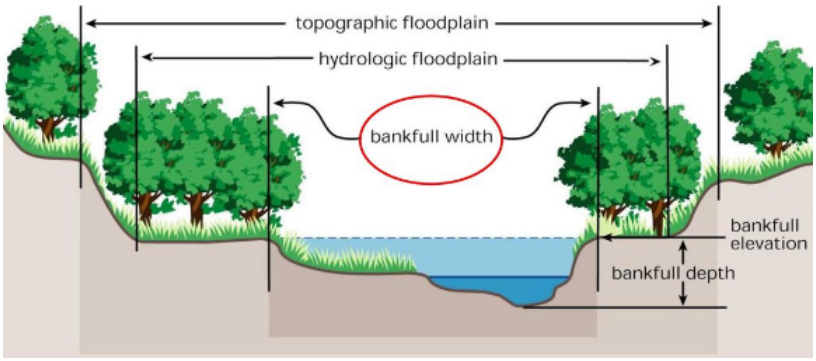

Figure 4.4: Bank-full Width: The width of a channel before it overflows its bank.

It is not an easy task to predict the bank-full width increase (and consequently, the need for culvert reconstruction) as a function of changes in precipitation patterns. For this study, the approach was to segment the need for culvert reconstruction with the occurrence of heavy rain storms. We assumed that culverts must be reconstructed at full cost (before being used again) if a historical *100 year 24-hour* event occurred in their area. An n-year event is

something that is expected to occur every n years, which is equivalent as saying that has a yearly probability of occurrence of $\frac{1}{n}$. A *100 year 24-hour* rainfall is an event where the total precipitation that falls in a given year, in a 24-hour period, exceeds the current 99^{th} percentile of 24-hour precipitations. This is equivalent as saying that the *maximum* 24-hour precipitation in a given year is bigger than the 99^{th} percentile. In this paper, we assume that road segments with culverts will fail in a future decade t if during that decade, the max. 24 hour precipitation exceeds the historical 99^{th} percentile value (referred from now on as $V_{\text{hist-99}}$), where we are assuming that this failure comes from the fact the culvert infrastructure is not able to hold events of this magnitude.

In the previous section we described the new road cost structure imposed by extra erosion. Instead of having a linear decay as a function of time, road segments are assumed to degrade with time but also with an extra rate proportional to the annual precipitation. In addition to this effect, the ARDM assumes that road segments with culverts can suffer from failure due to extreme events that have the potential to exceed the capacity of culverts to relieve upstream flow. The next example shows how road failure due to extreme events were incorporated in the ARDM's cost structure: Let's take a road segment i that has culvert(s) and was just reconstructed to standard/local conditions. This road segment will have a lifespan of 20 years until needing a new full reconstruction. Now, let's imagine that in the first decade since its reconstruction, a *100 year 24-hour* storm affects the area where this road segment is located. Instead of having a lifespan of 20 years, this lifespan is reduced to 10 years since the road segment is assumed to be completely destroyed (in the sense that *i's* culverts are not able to hold an event of this magnitude and therefore the road segment needs a full reconstruction before being used again for hauling).[4]

Now, the climate projections built for this study only provide the probability of extreme event occurrence in every decade, not the actual occurrence. Continuing with the previous example, we can't be sure about the actual failure of road segment i in a particular decade, and consequently, we don't know if this road needs a new reconstruction after 10 or 20 years. Nevertheless, we can calculate the *expected* lifecycle of road segment i with the following formula:

$$\textit{Expected Lifecycle}_i = 10p + 20(1-p) \tag{4.2}$$

where p is the probability of storm occurrence during the first decade after its last reconstruction.

Using the same argument as in the previous section, because the law requires that roads are reconstructed to standard/local conditions (meaning that roads last 20 years before needing a new full reconstruction), the new standard full cost of reconstruction, which considers the probability of *100 year 24-hour* events and higher erosion rates, for any road segment i is:

$$\textit{Final\_}\, C_i = \hat{C}_i \cdot \frac{20}{10p_i + 20(1-p_i)} \tag{4.3}$$

[4]For modelling purposes, we assume that climate effects are only seen at the end of the decade. This means that although the storm event could have destroyed the culvert in the first 5 years since its reconstruction, the road can be considered to be functional during the complete decade, this is why a road failure in the first decade still translates into a 10 year lifespan.

where $\hat{C}_i$ is the previously calculated full reconstruction cost that only considers faster decay due to higher erosion rates. Notice that if the road segment has no culverts, then p_i=0, which means that $Final\_\, C_i = \hat{C}_i$.

4.3 ARDM Cost Structure Summary

In this new model, roads are assumed to degrade in 20 years, but not in a linear way. Their decay is a linear function of time but it is accelerated by higher erosion rates and storm events. In order to avoid accelerated decay, a decision maker can preemptively build more robust and expensive structures that are able to withstand the future 20 year precipitations and storms. If the DM doesn't do so, the state will eventually charge him/her for the extra maintenance costs if the climate behaves in a more aggressive way than expected (and the state will pay if it happens the other way around) by adjusting the OF.

The full reconstruction cost of a road segment i in period t, that expects a future extra precipitation of $x_{i,t,t+1}$ % in the next 2 decades, and has a probability of storm occurrence of $p_{i,t}$, is:

$$Final\_\, C_{i,t} = C_i \cdot (1 + \frac{2x_{i,t,t+1}}{100}) \cdot \frac{20}{10p_{i,t} + 20(1 - p_{i,t})} \tag{4.4}$$

Following the same structure as the EFCM, this model has 2 cost tiers: road segments that were reconstructed 10 years ago can be reconstructed at half the full cost (half of $Final\_\, C_{i,t}$), while road segments that have not been reconstructed in 20 years or more need a reconstruction at full cost before being used again for hauling.

Chapter 5

Data

In this chapter we describe the data used to build the new road reconstruction cost scenarios. These scenarios were build using **Climate Data** from the Climate Model Inter-comparison Project and **Forest and Road Data** provided by the Washington State Department of Natural Resources (DNR). The climate data, consisting of hourly precipitation rates from 2010 until 2100, was used to build erosion and storm event predictions for the century, which were projected over the forest and road network data to build the new reconstruction costs scenarios.

5.1 Climate Data

Future precipitation can be predicted by climate models, which give projections of future atmospheric conditions and their uncertain behaviour. Even though many models are used for this purpose, General Circulation Models (GCMs) are the most consistent at incorporating the increasing greenhouse gas concentrations in their regional climate estimates (IPCC, 2018). GCMs are highly sophisticated mathematical models that use a set of physics equations in order to run computer simulations for weather forecasting and understanding climate change. 12 GCMs, obtained from the international Climate Model Inter-comparison Project, phase 5 (CMIP5; Taylor et al. (2012)) were used for this study (Table 5.1):

Model	Center
ACCESS1-0	Commonwealth Scientific and Industrial Research Organization (CSIRO) Australia/Bureau of Meteorology, **Australia**.
ACCESS1-3	Commonwealth Scientific and Industrial Research Organization (CSIRO) Australia/Bureau of Meteorology, **Australia**.
bcc-csm1-1	Beijing Climate Center (BCC), **China** Meteorological Administration.
CanESM2	**Canadian** Centre for Climate Modeling and Analysis.
CCSM4	National Centre of Atmospheric Research (NCAR), **USA**.
CSIRO-Mk3-6-0	Commonwealth Scientific and Industrial Research Organization (CSIRO)/Queensland Climate Change Centre of Excellence, **Autralia**.
FGOALS-g2	LASG, Institute of Atmospheric Physics, **Chinese** Academy of Sciences.
GFDL-CM3	NOAA Geophysical Fluid Dynamics Laboratory, **USA**.
GISS-E2-H	NASA Goddard Institute for Space Studies, **USA**.
MIROC5	Atmosphere and Ocean Research Institute (The University of Tokyo), National Institute for Enviormental Studies, and **Japan** Agency for Marine-Earth Science and Technology.
MRI-CGCM3	Meteorological Research Institue, **Japan**.
NorEXM1-M	Norwegian Climate Center, **Norway**.

Table 5.1: Global Climate Models used for this project.

These models were selected by the Climate Impacts Group (University of Washington) from a pool of candidates using 40 performance metrics aimed at identifying models that best capture the dynamics governing large-scale precipitation in the PNW. The selection criteria identified the GCMs that minimize the difference between predicted and observed historical values for these key performance metrics. Some of these metrics were:

- **SLP spacecorr:** Seasonal average sea level pressure, averaged over each domain. Difference between simulated and observed.
- **tas_bias:** Average surface temperature, 1960-1999. Difference between simulated and observed.
- **PRW95 spacebias:** Winter (December-February) 95th percentile of daily precipitable water, averaged over the Nearshore Pacific Northwest domain. Difference between simulated and observed.

Next, Fig. 5.1 shows all metrics evaluated by the CMIP5 for every GCM[1], ranging from 0 to 1, where 0 (blue) represents perfect prediction and 1 (red) means highest bias:

[1]ACCESS1-3 is missing in Figure 5.1 as it was developed after CMIP5.

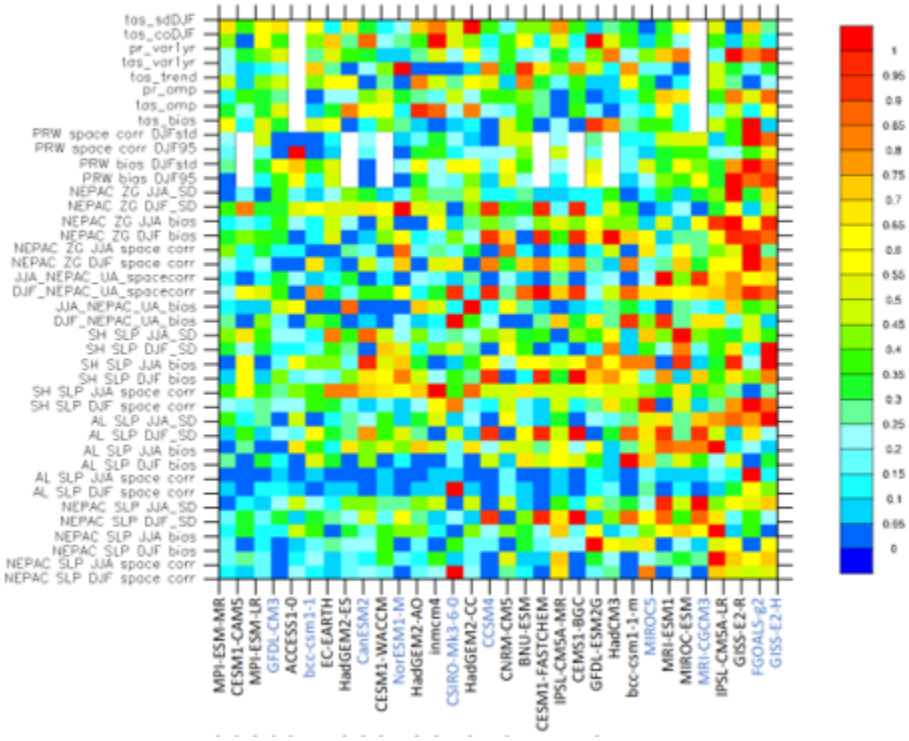

Figure 5.1: Relative error of each metric (y-axis) (normalized to range from 0 to 1) for each GCM (x-axis). Models are ordered left to right in ascending mean relative error.

As it was mentioned earlier, GCMs are designed to interact with future changes in greenhouse gas concentrations. Because gas emissions depend on so many factors such as economic growth, political regulations and social factors, it is very difficult to predict their behavior, and so the quality of climate model predictions gets compromised. One approach that climate scientists have used to solve this issue has been considering only a small number of possible greenhouse gas scenarios, which can be achieved by different combinations of political and technological actions. By doing so, there is no need to predict future emissions with high precision, it is sufficient to just predict a specific greenhouse gas scenario and couple it with a GCM.

In 2014, The Intergovernmental Panel for Climate Change (IPCC) identified four scenarios to cover the range of plausible gas emission trajectories that could be observed in the future. These scenarios, called Representative Concentration Pathways (RCPs) and developed by Van Vuuren et al. (2011), differ by their continuous change in CO_2 emissions and concentration, as it can be seen in Table 5.2:

Current scenarios	Concentration in 2100 (ppm CO_2-eq)	Change in annual CO_2-eq emissions (% of 2010 emissions)		*Description*
		2050	2100	
RCP 2.6	430-480	-72 to -41%	-118 to -78%	*"Very Low"*
RCP 4.5	580-720	-38 to +24%	-134 to -21%	*"Low"*
RCP 6.0	720-1000	+18 to +54%	-7 to +72%	*"Moderate"*
RCP 8.5	>1000	+52 to +95%	+74 to +178%	*"High"*

Table 5.2: Four Representative Concentration Pathways. This table shows the target concentration in 2100 and the percent change in annual emissions, relative to 2010, for both 2050 and 2100. These concentration values consider every greenhouse gas, but it is expressed in "CO_2-equivalent" to show an equivalent warming potential (IPCC (2014)).

The data for this study was provided by Guillaume Mauger from the CMIP5 and Cliff Mass from UW Atmospheric Sciences, and consists of precipitation projections from a total of 12 GCMs coupled with the 8.5 RCP concentration pathway, also referred to as the *business as usual* scenario since its growth in emissions is similar to past decades. Although we were forced to use this RCP because it was the only data available when we started the project, assuming the *worst case* climate scenario is often a useful and accepted practice in the forest industry. It also addresses one of the questions of this study, which is to understand the potential damage of ignoring climate change in harvesting and road (re) construction planning.

The actual data came from Regional Climate Models (RCMs) instead of GCMs, which are more precise estimates that can describe local changes in rain storms and climate in general. GCMs serve as boundary conditions to build the RCMs, and they are necessary because local climate patterns can be influenced by conditions in other parts of the globe, ones which can only be captures by high resolution models such as GCMs. The reason why RCMs were used instead of GCMs is that although the latter are good at providing large scale climate predictions and representing key aspects of atmospheric rivers (e.g., Flato et al. (2014)), their low resolution sometimes fails to capture how local differences in orography[2] in the Pacific Northwest alter the precipitation patterns and intensity.

An example of this phenomenon is the interaction between atmospheric rivers and the mountains of the coast of the PNW, which would be difficult to capture without the precision of RCMs. An atmospheric river is a narrow current of warm, moist air from the tropics and subtropics that extends northward into the midlatitudes (Fig. 5.2), and it is the new unusual direction in which its approaching the PNW's coasts one of the most plausible reasons that explain the observed increase in heavy storms (Mass, 2020).

[2]Orography: the branch of physical geography dealing with the formation and features of mountains.

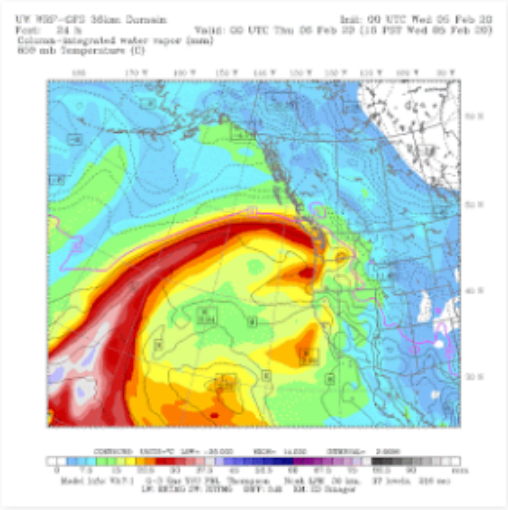

Figure 5.2: Atmospheric River Simulation approaching the PNW coast from the west (Mass, 2020)

But, why is this unusual direction causing an increase in precipitation storms? One of the reasons is that this westerly wind moves rapidly up the mountains, cooling and releasing large amounts of water vapor in the atmospheric river which later on condenses and is transformed into liquid water. Atmospheric rivers in the past came from south to north with not much upslope flow since the air was running parallel to the terrain, avoiding this increased water vapor phenomenon.

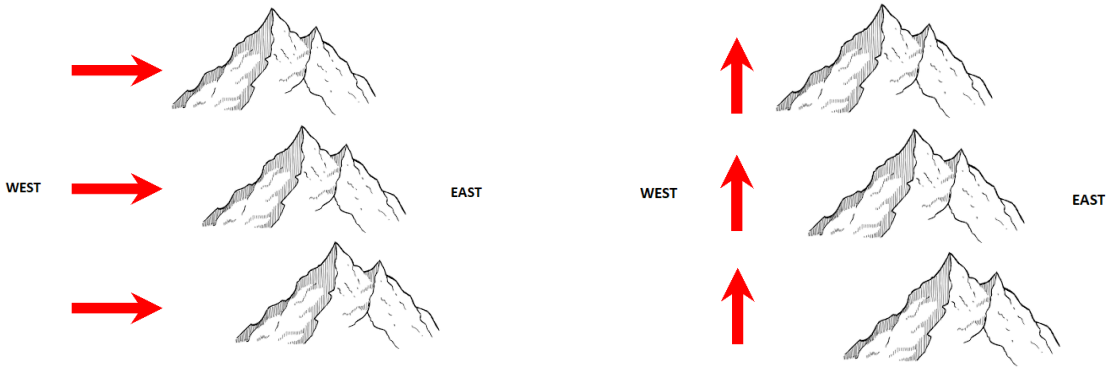

(a) Horizontal ARs

(b) Vertical ARs

Figure 5.3: West-East (a) vs. South-North (b) Atmospheric Rivers. Compared to (b), (a) produces heavier rains due to a faster elevation of water vapor over the mountains.

Mass and Mauger's 12 projection simulations were performed using the Weather Research and Forecasting (WRF[3]; Skamarock et al. (2005)) community mesoscale model for each RCM, using the 12 previously mentioned GCMs as boundary conditions for each one. These projections gave hourly precipitation outputs on a curvilinear 12-km grid for the Pacific Northwest, from the years 1970 until 2100. We used their hourly precipitation outputs to

[3] `https://www.mmm.ucar.edu/weather-research-and-forecasting-model`

build projections of future soil erosion and storm probability over the forest road network. These projections were used to build 27 scenarios of future road reconstruction costs, which were a function of extra soil erosion (caused by annual extra precipitation) and increasing storm probability (caused by large 24 hour rains). These new road reconstruction costs, which have an endogenous structure (they depend on the time since the last reconstruction) and also vary upon external factors (total precipitation and storms) are one of our main contributions to science, together with the ARDM stochastic model we built to solve the harvest schedule problem taking these scenarios into consideration. The workflow and methods used to build these precipitation projections and road reconstruction costs scenarios are described in detail in the next chapter 6: Climate Data Processing and Scenario Generation.

5.2 Forest and Road Data

The Olympic Experimental State Forest (OESF) was chosen as the case study forest for this project. The Washington State Department of Natural Resources manages state trust lands in the OESF, to generate a sustainable flow of revenue to counties, universities and other state trust land beneficiaries. Streams in the OESF support robust populations of salmon at a time when many Northwest salmon runs are losing strength. In the OESF, DNR balances the two objectives by implementing an experimental approach called "integrated management".

The OESF is managed for both revenue production and ecological values, rather than separating state trust lands into large areas managed for a single purpose. This is achieved through innovative silvicultural techniques, landscape-level planning, intentional learning through research and monitoring, and application of new information to management through a formal adaptive management process. In 2009, the OESF joined the Experimental Forest and Range Network (EFRN), in an agreement between DNR and the U.S. Forest Service Pacific Northwest Research Station that encouraged collaboration between OESF and Forest Service scientists.

Silviculture and fish research has been conducted on state trust lands on the western Olympic Peninsula since the 1970s. After the designation of the OESF in 1992, it intensified and broadened to cover forest and wildlife ecology, geology, and riparian [4] management among other topics. The majority of the past research and monitoring activities are listed in the OESF Research and Monitoring Catalog, published by DNR in 2008 with many recently completed and ongoing projects.

One of the goals of our work was to show how our model could be applied to the Upper ClearWater landscape of the OESF. The Upper ClearWater is a major river drainage (watershed) of the OESF which has a rich history of scientific investigation. Thus, a new forest planning model formulation applied to the Upper ClearWater that includes the impacts of climate change on road connectivity would make my findings meaningful.

Road network and forest stands data was provided by the Washington State Department of Natural Resources (DNR) for the Olympic Experimental State Forest (OESF). These data include important aspects of the forest and road network such as tree and site potential infor-

[4] Riparian: Relating to or situated on the banks of a river

mation (the average tree species harvested in this area are Douglas fir and western hemlock[5]), road segment information, distribution of forest management units (FMUs), attributes such as road proximity to streams and also their connectivity to FMUs.

Fig. 5.4 shows a map of Washington State (green points) with the OESF road network at the upper left corner (blue). Fig. 5.5 (a) shows the same road network (blue) but identifying segments that have at least one culvert (red). Finally, Fig. 5.5 (b) shows the road network (blue) and its connectivity to the different FMUs (yellow polygons).

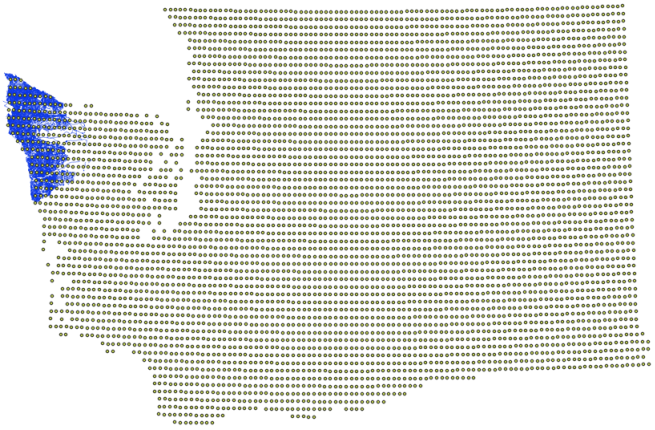

Figure 5.4: Washington State (green) and OESF road network (blue).

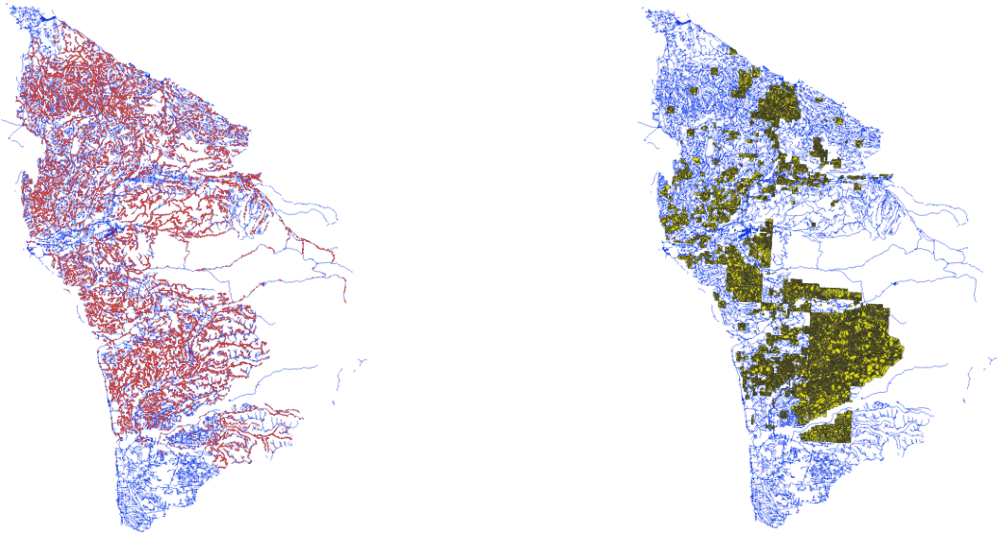

(a) Roads (blue), segments with culverts (red).

(b) Roads (blue), FMUs (yellow).

Figure 5.5

[5]Douglas fir is the largest and tallest member of the pine family, and is the most widely used wood for building and construction. Western hemlock on the other hand, is a type of hemlock also used construction, roof decking and plywood.

The road network shown above extends to a total area of 4.450 km^2 and has 5.532 FMUs that cover a total area of 1.095 km^2 (270.580 acres). It is made up of 26.348 road segments with a total length of 10.104 km., and an average length of 383 m. Out of the 26.348 road segments, 12.249 (46%) have culverts, with an average of 9 culverts per road segment.

Because the goal of this work is to understand how the ARDM can accommodate the impact of future climate change on the road network, having future climate data over each road segment for every year in the planning horizon was mandatory. To assign the corresponding climate information to every road segment, a spatial join was done between the road network and the yearly climate projections data. These climate data projected over the PNW was partitioned into 49 climate grid cells with a 12km resolution, so two different road segments inside the same climate cell were associated with the same climate data.

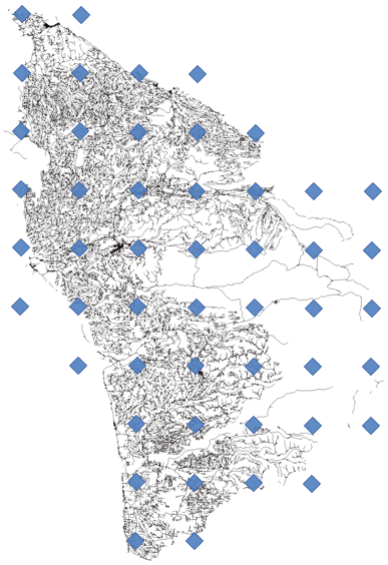

Figure 5.6: Road network and RCM grid cells centers (blue squares).

After trying different approaches to test the ARDM in this area, we realized that the instance size was too big, and the computational burden of applying a stochastic model was immense. The initial instance was tested using IBM ILOG CPLEX 64-bit 12.9.0 on an MSI GP62MVR 7RFX Server with an Intel(R) Core(TM) i7-7700HQ CPU @ 2.80GHz (eight processors) with 24 GB RAM and the Ubuntu 18.04.01 Server 64-bit operating system, and after 10 hours of computer running time, the model only reached a 5% MIP gap.

Reaching a very low gap was crucial for this project for the following reason: The objective function of a stochastic problem (OF) is made up of the weighted average of the objective functions OF_s of each scenario s. Let's assume that the model is solved up to a 5% gap. Now, consider 2 scenarios, s_1 and s_2, that only differ in the last 3 decades. Because of the discount rate, the coefficients for these 3 final decades are very small and have little impact in the OF, and therefore OF_{s_1} and OF_{s_2} are practically identical.

When the stochastic model is solved, the 5% gap hides this small difference between OF_{s_1} and OF_{s_2}, and it is very likely that we end up with identical solutions for both scenarios s_1 and s_2 even thought they are different in 30% of the decades[6]. Because part of the goal of this project is to analyze the different harvesting and road reconstruction strategies under every scenario, only a very small gap must be allowed in order to avoid the problem of having identical solutions for two different scenarios.

After analyzing other possible areas of the OESF that were smaller and therefore could be solved to optimality in a reasonable time, we ended up working with a landscape located on the Sol Duc River drainage area in the North part of the OESF. This area is circled in red in Fig 5.7, followed by a close up in Fig 5.8:

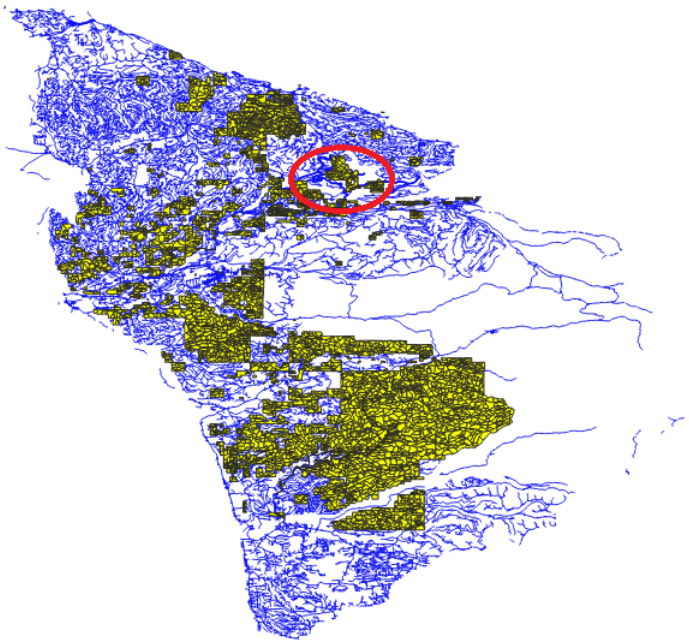

Figure 5.7: Sol Duc River drainage.

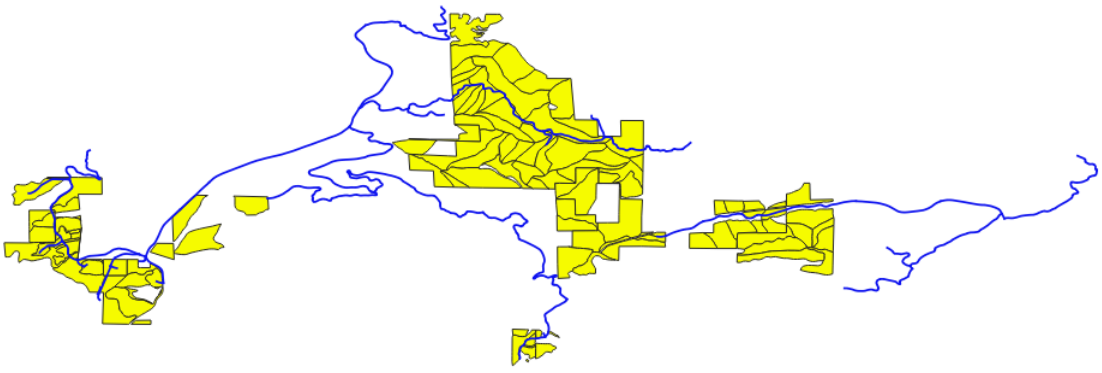

Figure 5.8: Sol Duc River drainage road network and FMUs.

[6]The coefficients of the ARDM are multiplied by $z_t = (1 + \frac{r}{100})^{10(1-t)}$ where r is the discount rate and t is the decade. With $r = 0.05$, $z_8 = 0.03$, $z_9 = 0.02$ and $z_{10} = 0.01$, i.e. very small coefficients.

This location is a 150 km^2 forested land-base, with 98 FMUs covering a total area of 17km^2 (4200 acres), which is covered by 4 RCM climate grid cells. This area has an infrastructure of 65 road segments that add up to a 63.5 kilometer road network, with an average length of 976 m. (min=13 m., max=4.2 km.). Out of the complete network, 53 of the road segments have culverts (82%), with an average of 15 culverts per road segment (min=1, max=73), adding up to a total of 821 culverts. The next image shows the road segments with culverts in red, and the ones without, in blue:

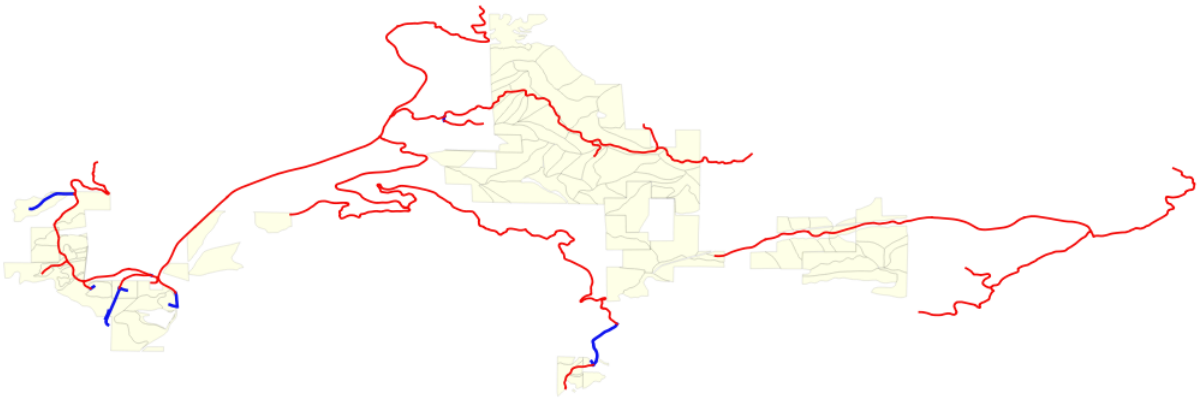

Figure 5.9: Road with culverts (red), and without (blue)

The Sol Duc River drainage is much smaller than the Upper ClearWater area that we first considered. After doing a couple of test in this new location, we decided that this was an appropriate OESF area to test the ARDM, mainly because the model could find close to optimal solutions after a reasonable computational time (which as it was mentioned before, was crucial to identify differences in harvesting and reconstruction strategies for different scenarios). Finally, it should be pointed out that due to the size of the area, even flow constraints (constraints 3.1e and 3.1f of the Model II formulation) and the average ending constraints (3.1g) were eliminated from the new model because they were not necessary, as these constraints only apply to big forests. 3.1e and 3.1f constraints ensure a uniform flow of wood to meet demand variations and is also particularly important for communities whose stability can be assured only by the steady and continuous flow of raw materials from the forest resources. Nevertheless, this only applies to the complete forest, it does not apply independently to particular zone or unit. A forester could decide it is in his/her best interest to completely harvest a zone in a particular decade without touching it in the previous ones, something that is permitted as long as the total harvest across all the FMUs is within 25% from the previous decade. Because the area for our project is small, it can be considered as a small zone inside the complete OESF forest landscape, and therefore constraints 3.1e and 3.1f do not apply. The same happens with constraints 3.1g: They only apply to the whole forest as a unit, not for a particular zone.

Figure 5.10: Sol Duc River on the Olympic Peninsula in Olympic National Park, Washington.

The next chapter describes the process of taking the 12 RCMs precipitation outputs, transforming them into extra erosion and extreme event probability realizations and then creating 27 new road reconstruction scenarios.

Chapter 6

Climate Data Processing and Scenario Generation

This chapter describes the series of steps at creating the set of 27 road reconstruction costs *scenarios* that were used to build the *Scenario Tree* to test the ARDM. These scenarios are a sequence of 10 climate intensities for each decade along the planning horizon, which are then translated into new road reconstruction costs. This new road reconstruction costs were built by projecting *Extreme Event Probability Realizations* and *Extra Erosion Realizations* over the Sol Duc River area's road network. The first section of this chapter, **Climate Data Processing**, shows how the climate data was processed in order to build erosion and extreme event realizations of different intensities, and how these were translated into the new road reconstruction costs realizations. The second section, **Scenario Generation**, describes how these new road reconstruction costs realizations were translated into the 27 different scenarios.

6.1 Climate Data Processing

Having hourly precipitation projections from 1980 until 2100 for every Regional Climate Model was the first step at creating future road reconstruction cost realizations. It should be made clear that for this project we assumed that climate only affect these costs, but has no effect on tree growth or yield. Harvesting adaptation strategies under stochastic tree growth and yield has been thoroughly studied by other researchers (e.g. Garcia-Gonzalo et al. (2020)), that is why we decided to leave it outside the scope of this project and focus on a new effect.

These next sub-sections describe the series of steps followed in order to create *Extreme Event Probability Realizations* (1) and *Extra Erosion Realizations* (2) for each decade.

6.1.1 Extreme Event Probability Realizations

Future storms were modeled as the occurrence of historical *100 year 24-hour rainfall events*, which are 24-hour rainfalls bigger than the historical 99^{th} percentile. The historical probability (1980-2009) of a 24-hour rainfall being bigger the historical 99^{th} percentile value ($V_{\text{hist }99}$), is equal to 0.01 (by definition) because it is a 100 year event and therefore has a probability of $\frac{1}{100}$ =0.01. However, if future precipitations become more intense, then the distribution of total precipitation of 24-hour rains, and consequently max. 24-hour rainfalls, will change and shift to the right, as shown in Fig 6.1. This potential shift will increase the probability of future yearly max. 24-hour rains being bigger than $V_{\text{hist }99}$, and therefore, in the context of our model, give more frequent storms with culvert destruction potential. As it was mentioned in section 4.2, the ARDM does not model the actual occurrence of extreme events, it only takes into account the new probability of these eventualities taking place and builds on it to create new road reconstruction costs.

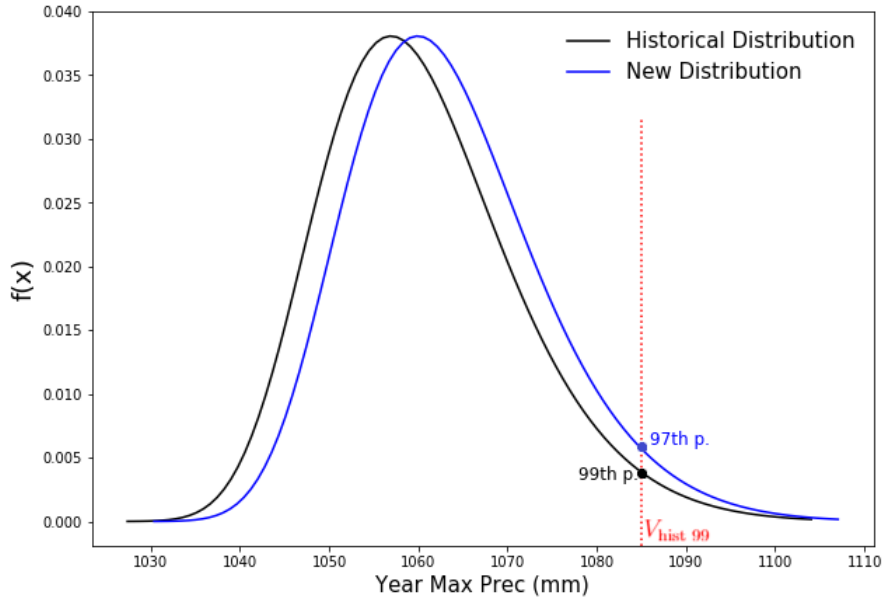

Figure 6.1: For the historical yearly max. 24-hour precipitation distribution (black), $V_{\text{hist }99}$ corresponds to its 99_{th} percentile. On the other hand, for a new and more intense precipitation distribution (blue) that has shifted to the right, $V_{\text{hist }99}$ only corresponds to the 97_{th} percentile, meaning that it corresponds to a more frequent $\frac{100}{3} \approx$ 33-year event.

Next, we describe the steps at creating Extreme Event Probability Realizations for each road segment in every decade.

1. **Tridecades:**
   Estimating the distribution of yearly max. 24 hour precipitations requires consecutive year data in order to make the proper calculations. Using 30-year periods is an appropriate length of time for estimating the distribution of yearly max. 24 hour rains because it is roughly long enough to encompass natural variability and to calculate extreme statistics (Mauger et al., 2018). As a consequence and for modelling purposes, every year in the 30-year sample data has the exact same distribution for max. 24-hour precipitations. For this project, the planning horizon was divided into 3 30-year peri-

ods and 1 40-year period, referred from now on as *tridecades*[1]. Years 1980-2009 were assigned to the *Historical Tridecade*, 2010-2039 were assigned to the *First Tridecade*, 2040-2069 were assigned to the *Second Tridecade*, and years 2070-2109 correspond to the *Third Tridecade* (the last tridecade is made of 4 decades instead of 3 because it is more common to build a 10-period planning model rather than a 9-period one, and 3-30 year tridecades would only add up to a total of 9 decades.). The following steps describe how we calculated the new yearly max. 24 hour precipitation distribution for each tridecade, and consequently, the associated probability of storm occurrence for the tridecade and every decade in it. As it was previously mentioned, given that tridecades are 30-year periods and the decision periods for the model are decades, each decade inside a tridecade was associated with the same storm occurrence probability[2].

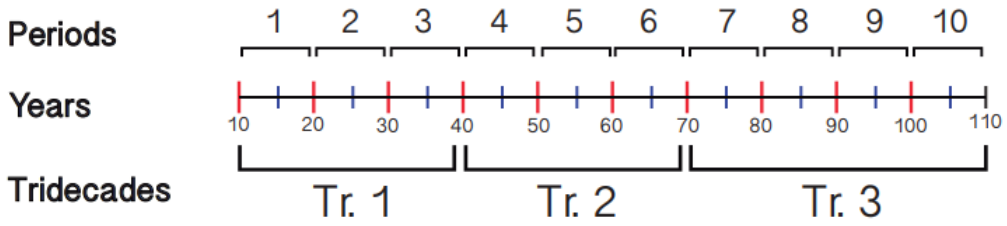

Figure 6.2: Relation between periods, years and tridecades. Periods, or decades, have a length of ten years, and the first one starts in the year 2010. The first 3 periods are part of the *First Tridecade* (Tr.1), periods 4, 5, 6 are part of the *Second Tridecade* (Tr.2) and periods 7, 8, 9 and 10 are part of the *Third Tridecade* (Tr.3). Harvesting and road reconstruction decisions are assumed to occur at the beginning of every period (red marks), and the climate is assumed to manifest itself at the middle of every period (blue marks).

2. **Yearly Max. 24-hour Precipitations:**
   To calculate the extreme statistics of future rainfalls, the yearly max. 24-hour precipitation of every year was calculated for each grid cell under each RCM. This was an easy task given that we already had the hourly precipitation for each year.

3. **Fitting a Distribution:**
   With the max. 24-hour precipitation for each year inside a tridecade, Extreme Value Analysis (EVA) was used to find a function to represent the distribution of yearly max. 24-hour rains. EVA is a branch of statistics that deals with probability distributions of maximum values of a sample. What it does is it seeks to assess the probability of events that are more extreme than any previously observed, and has many applications such as estimating the probability of unusually large floods, side effects of drugs, large wildfires, economical crisis, and for this study, yearly max. 24-hour rains. Using EVA as a framework, we selected a set of functions from the Generalized Extreme Value Distribution[3] and used them to try and fit the empirical data of yearly max. 24-hour

[1]Tridecade is the result of combining the words "three" and "decade" into one word (the last period consists of "four" decades, but it will also be referred a tridecade for simplification).

[2]Because there was no climate data for the 10^{th} period (years 2099-2109), it was assumed that it was identical to the previous decade.

[3]GEV: Family of continuous probability distributions that combines the Gumbel, Weibull and Frechet distributions, and is commonly used to model extreme events

precipitations. Having these extreme rains being represented by a known distribution allowed me to calculate the probability of any storm being bigger than any given value.

To get an initial understanding of the behaviour of yearly max. 24-hour precipitations, the first step was to use a graphical test for some grid cells, tridecades and RCMs, and see if they their empirical distribution could be approximated by known functions. Fig. 6.3 shows the empirical frequency (divided into 10 bins) of max. 24-hour precipitation for one particular grid cell during the *First Tridecade* under RCM Access1.0-RCP8.5, along with 6 known theoretical probability density functions[4].

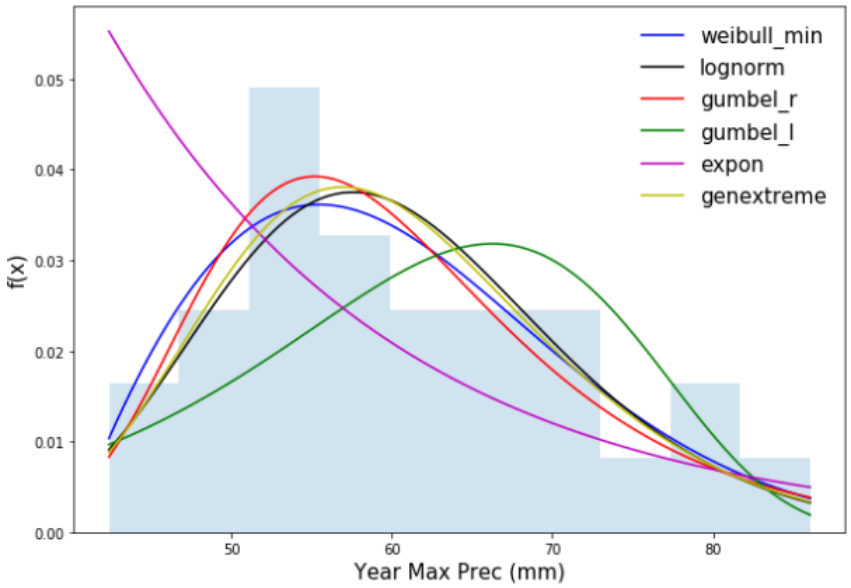

Figure 6.3: Empirical yearly max. 24-hour precipitation frequency vs. 6 known theoretical density functions: Weibull Min., Log-Normal, Right-Gumbell, Left-Gumbell, Exponential and Generalized Extreme Value Function.

As it can be seen in Figure 6.3, all theoretical distributions show a good fit except for the Exponential and the Left-Gumbel function. CDF and QQ-plot graph tests were also performed in several combinations of RCM-cell-tridecade to asses the quality of fit of these 6 known density functions (Appendix B and Appendix C). These tests confirmed that these distributions were good candidates for modelling the max. 24-hour precipitations for every RCM-cell-tridecade.

4. **Analytical Goodness of Fit:**
   Because the precipitation data for every trio of RCM-tridecade-grid cell does not necessarily follow the same distribution, an algorithm was executed to find the function that best fit the empirical data of each one of them. The 6 distributions were evaluated for each trio and were graded by the AIC criterion: the distribution with lowest AIC was chosen to model the max. 24-hour precipitation for that particular RCM-tridecade-gridcell.

[4]Maximum Likelihood Estimator (MLE) was used to calculate the optimal parameters that best fit the empirical data, for each one of the theoretical distributions.

5. **Historical 99^{th} percentile:**
   For every grid cell, the historical yearly 24-hour 99^{th} percentile value ($V_{\text{hist }99}$) was calculated from the previously found theoretical distribution.

6. **New Storm probabilities for each RCM:**
   Using the best fitting distribution found in (4) for every RCM-tridecade-grid cell, the quantile function was applied to calculate the new probability of a yearly max. 24-hour precipitation being bigger than the $V_{\text{hist }99}$ value. Figure 6.4 shows the average % change of the historical probability of storm occurrence over tridecades across all grid cells under each RCM:

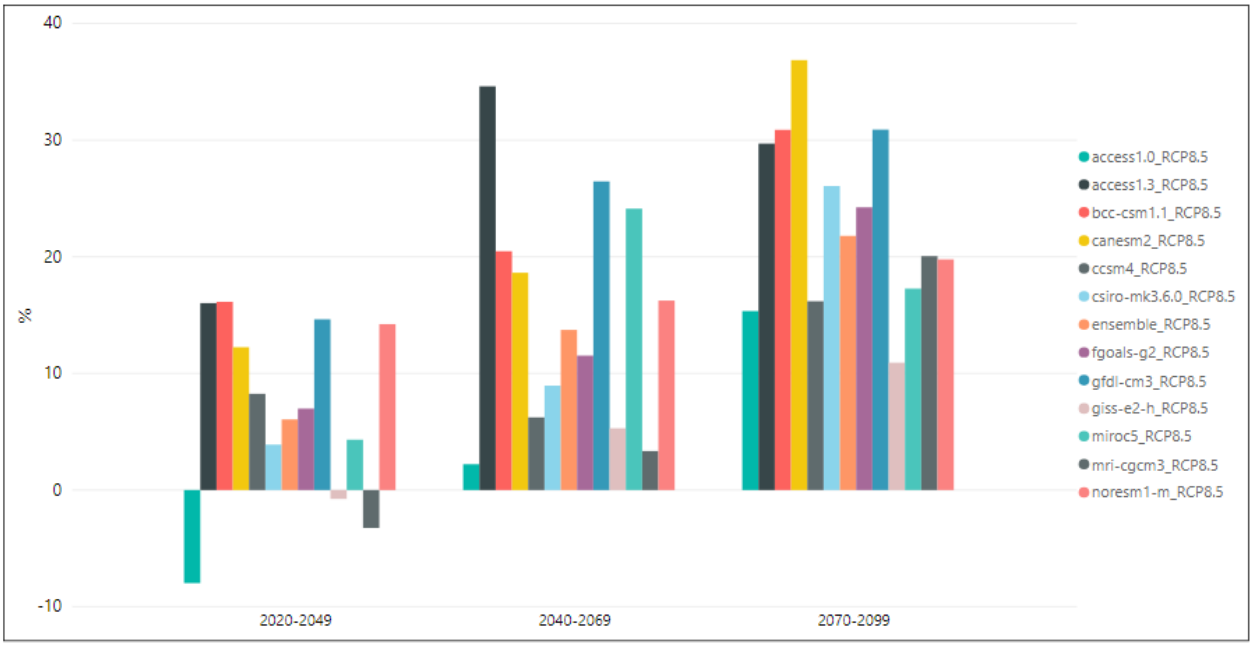

Figure 6.4: Average % change in probability of storm occurrence (year max. 24-hour precipitation being bigger than the historical 99^{th} percentile) compared to the historical p=0.01 value, across all grid cells for every tridecade under the 12 RCMs (each color represents a different RCM).

Although the results differ across RCMs, there is a clear tendency towards an increasing storm occurrence probability as we move through the century. This graph corroborates what the scientific community predicts for future years regarding the increase in heavy rains over the PNW. Finally, the new storm probability value of each of the 12 RCMs, for every tridecade-grid cell combination, was stored in a quantiles vector named $Q_{(tridecade,grid\ cell)}$.

7. **Quantile Distribution:**
   The objective at this step was to fit a Normal distribution to the $Q_{(tridecade,grid\ cell)}$ vector for every tridecade-grid cell combination. The idea behind this was that later on, this Normal distribution would be divided into 3 intervals corresponding to three different levels of storm intensity. By modelling the quantiles vector as a Normal distribution, it can be divided in such a way that the left tail can be assigned to the *Low Storm*

Probability realization , the middle interval can be assigned to the *Moderate Storm Probability* realization, and the right tail can be the *Heavy Storm Probability* realization, each one corresponding to an increasing storm probability.

Because there are not enough data points to build a Normal distribution using the 12 quantile points in $Q_{(\text{tridecade},\textit{grid cell})}$, a Bootstrap method was used to fix this issue. The method consisted of sampling 12 values with replacement from $Q_{(\text{tridecade},\textit{grid cell})}$, calculating the average value, storing it in a *Replicates Vector*, and repeating this process 10.000 times. Now, this *Replicates Vector* follows a Normal distribution and it can be divided into the 3 intervals corresponding to the *Low* (left tail, weight=0.25), *Moderate* (middle section, weight=0.5) and *Heavy* (right tail, weight=0.25) storm probability realizations mentioned earlier, each one corresponding to a different probability of storm occurrence in a given year. Table 6.1 shows the average probability of storm occurrence in a given year inside a tridecade, where the average is calculated across every grid cell:

Tridecade	Low	Moderate	Heavy
1	0.022	0.031	0.039
2	0.039	0.044	0.056
3	0.034	0.050	0.067

Table 6.1: Mean yearly probability of storm occurrence over each tridecade under the *Low*, *Moderate* and *Heavy* realizations. The historical value of $p = 0.01$ should be used for comparison.

The following table shows more specific information on storm occurrence probability. While the previous table showed the storm probability in a given **year** inside a tridecade, the following table gives the storm occurrence probability in each **decade** under every storm intensity:

Intensity	1	2	3	4	5	6	7	8	9	10
Heavy	0.33	0.33	0.33	0.44	0.44	0.44	0.5	0.5	0.5	0.5
Moderate	0.27	0.27	0.27	0.36	0.36	0.36	0.4	0.4	0.4	0.4
Low	0.2	0.2	0.2	0.27	0.27	0.27	0.29	0.29	0.29	0.29

Table 6.2: Average Storm probability for every decade under every storm intensity. The historical value of $p = 0.096$ should be used for comparison.

Table 6.2 shows an increasing average probability of storm occurrence across grid cells as we move through the years, and that there is also a clear difference among different storm intensities.

The next figure is an example of how the storm occurrence probability is distributed across grid cells, for two different tridecades and storm intensities (the results for all combinations of storm intensity-tridecade can be found in Appendix D):

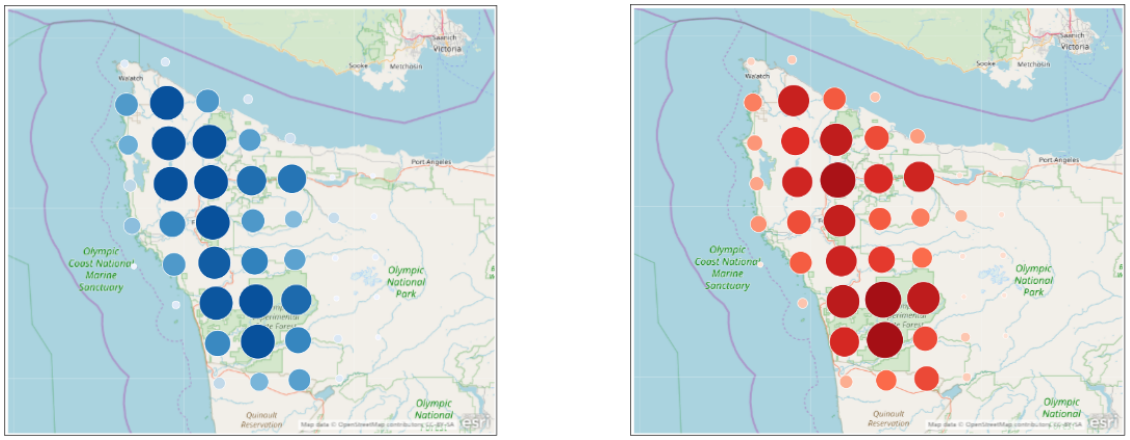

(a) Low Scenario, 2040-2069

(b) Heavy Scenario, 2070-2099

Figure 6.5: Yearly Probability of storm occurrence across grid cells, in different periods and storm intensities (bigger circles represent a higher probability).

For example, based only in these two storm intensity-tridecade pairs, we can expect a lower storm occurrence probability in the outer most part of the OESF area compared to the inside. It is also interesting to notice that the distribution does not show major differences for two different combinations of storm intensity-tridecade.

8. **Road segment realizations:**
   In order to assign a storm probability over each road segment of the network *with culverts* in each decade, which at this stage was only associated to the grid cells, a spatial join was performed between the climate and road network data layers as described in section 5.2: Forest and Road Data.

The process for calculating *Extra Erosion Realizations* for each road segment in every decade was a little bit easier, and very similar to the one just described for the *Extreme Event Probability Realizations*.

6.1.2 Extra Erosion Realizations

The next steps were followed to create Extra Erosion Realizations for each road segment in every decade.

1. **Historical Decade Precipitation:**
   To calculate Extreme Event Probability Realizations, the *Historical Tridecade* was set to the years 1980-2009 because as it was explained, a 30 year period was necessary to construct a yearly max. 24-hour precipitation distribution and calculate the $V_{\text{hist }99}$ value. For the Extra Erosion Realizations however, this was not necessary. To use the most recent information available, years 2000-2009 were used as a benchmark for decade total precipitation, and this value was later used to calculate precipitation increase in future decades for every combination of RCM-grid cell. Fig 6.6 shows the total precipitation from year 1980 until 2099, where the data for years 1980-2010 is the historical data and the values for years 2010-2099 are the average projection values calculated across all RCMs. Fig. 6.7 on the other hand, shows the average % change

in total precipitation for every decade under each RCM across all grid cells, while Fig. 6.8 shows the average % change over all RCMs.

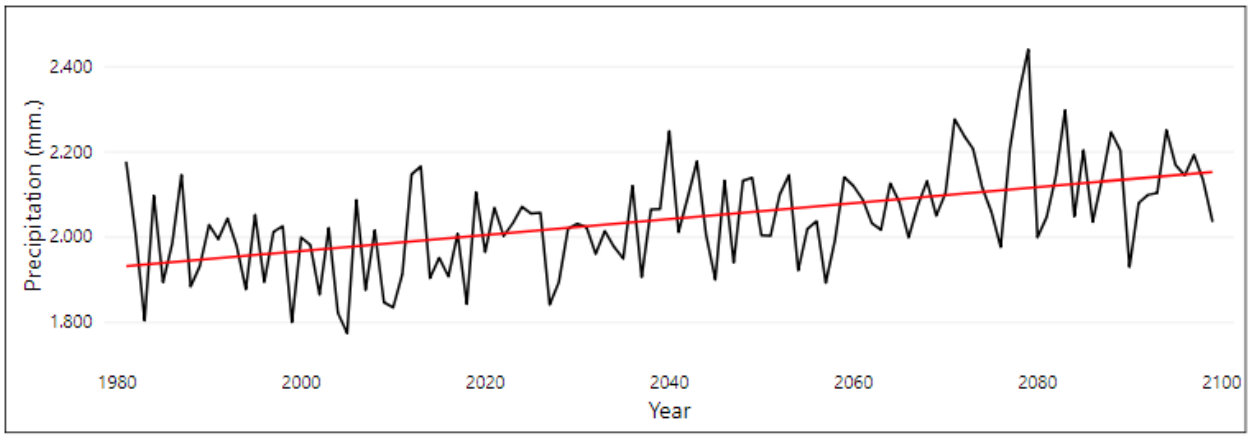

Figure 6.6: Average yearly total precipitation projections, calculated across the 12 RCMs.

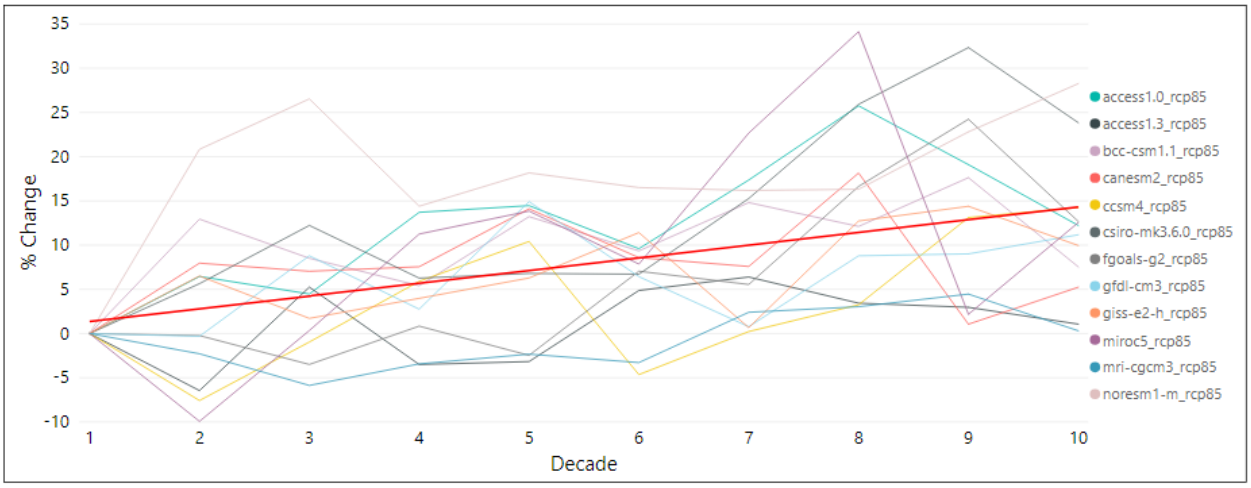

Figure 6.7: Average precipitation % increase for every decade compared to the historical years (2000-2009) under every RCM (Decade "0" correspond to historical years 2000-2009 that were used for comparison. Decade "10" is missing because as it was explained before, there is no climate information for years 2100-2109 and therefore it was assumed that its climate is identical to the previous decade (2090-2099)). Each transparent curve represents a different RCM and the red opaque line is the average tendency curve.

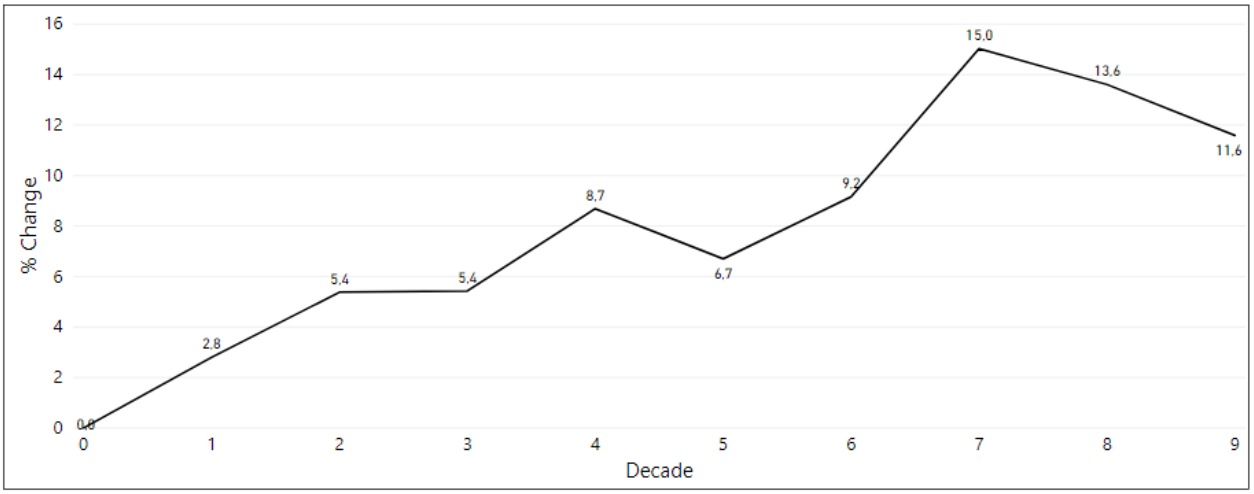

Figure 6.8: Average % change across all RCMs in every decade.

Fig 6.6 shows how RCMs predict an increasing tendency of total year precipitation over the PNW. Grouped by decade, Fig. 6.7 shows that, compared to the historical data (years 1980-2009), RCMs show different % total precipitation change projections for the future, but there is an increasing tendency as we move through the century. This conclusion is verified by Fig. 6.6, which shows an increasing average precipitation % change for future decades across all RCMs.

2. **Decade Precipitation Change:**
   For every RCM-decade-grid cell combination, the total projected precipitation was compared to the historical data. For every decade-grid cell pair, each one of the 12 RCM's precipitation % change was stored in a $Precipitation\ Change_{(decade,grid\ cell)}$ vector. Using the same bootstrap method described in the previous section, a Normal distribution of precipitation change was constructed with these $Precipitation\ Change_{(decade,grid\ cell)}$ vectors and was later on divided into 3 intervals, each corresponding to a different climate intensity: *Low*, *Moderate* and *High*.

   The next figure is an example of how the projected % change in total precipitation differs across the grid cells for two tridecades (the precipitation change heat map for every combination of decade-scenario over the OESF can be found in Appendix E).

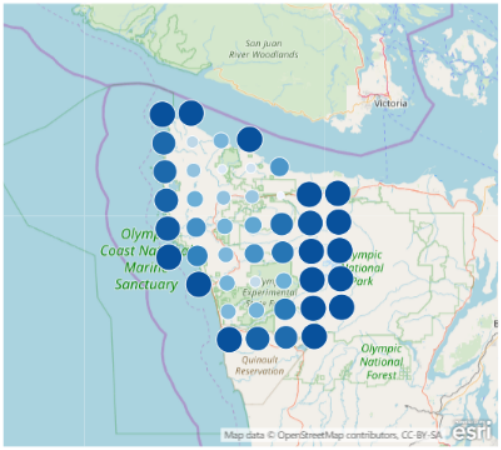

(a) Low Intensity, 2040-2049

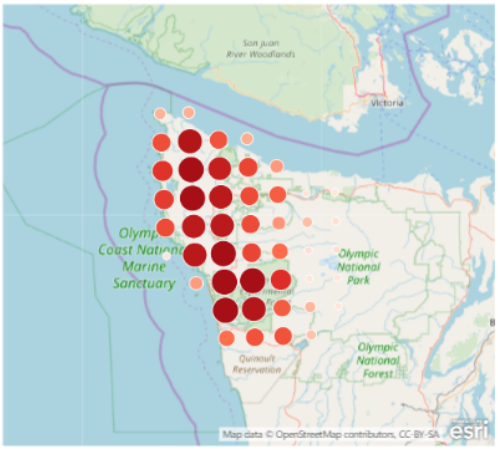

(b) Heavy Intensity, 2090-2099

Figure 6.9: Total precipitation % change, in different periods and different climate intensities. Bigger circles represent greater change compared to historical data.

For example, based only in these two tridecade-intensity pairs, we can can see a different distribution of precipitation change across the OESF when two climate intensity scenarios and decades are compared: (a) shows a bigger change in the outer most part of the forest, while (b) shows a bigger change in the inside.

Next, Table 6.3 shows the average erosion % change for every climate intensity. The erosion % change was calculated by multiplying the total precipitation change by a factor of 2, just as it was explained in chapter 4.1:

Intensity	1	2	3	4	5	6	7	8	9	10
Heavy	30	32	32	41	33	38	46	46	39	39
Moderate	5	9	9	16	11	14	25	22	17	17
Low	-22	-16	-16	-12	-14	-10	2	-4	-7	-7

Table 6.3: Average % change in erosion compared to historical data for every decade under every climate intensity.

Apart from the fact that more intense climates show a bigger change in erosion compared to historical data, it is also interesting that the erosion change curve grows and reaches its peak during the years 2070-2089, followed by significant fall in the last 2 decades.

3. **Road segment realizations:**
   Finally, in order to assign a decade precipitation change value (and therefore an erosion change value) to each road segment in the network, a spatial join was performed between the climate and the road network data layers.

6.1.3 New Road Reconstruction Cost Realizations

As it was described in the beginning of this chapter and also in chapter 4.3, Extra Erosion Realizations and Extreme Event Probability Realizations were combined to build New Road

Reconstruction Cost Realizations. When heavier than historical precipitations are expected, road segments have to be reconstructed at higher standards in order to last their usual life cycle (20 years). In addition to that, extra attention has to be paid to road segments with culverts, because increasing storm probabilities demand even more robust reconstructions capable of adapting to changes in channel morphology.

The new full reconstruction cost for every road segment i in every period t was calculated for the 3 possible intensity realizations $r \in [Low, Moderate, Heavy]$ using the following formula:

$$Final\_C_{i,t,r} = C_i \cdot (1 + \frac{2x_{i,t,t+1,r}}{100}) \cdot \frac{20}{10p_{i,t,r} + 20(1 - p_{i,t,r})} \tag{6.1}$$

This is the same formula as formula (4.4) in chapter 4.3, with the only difference that it now depends on the climate intensity index r. It is important to notice that this formula does not allow a different intensity for erosion change and storm probability: the expression regarding erosion ($2 \cdot x_{\mathrm{i},t,t+1,r}$) and the one for storm probability ($p_{i,t,r}$) share the same r index. This subtle detail is based on the assumption that erosion change is positively correlated with an increase in storm probability, which for our model, means that a realization of *Heavy* erosion change can only be coupled with a *Heavy* realization of storm probability (the same with *Moderate* and *Low* intensities). Although this may look like a natural assumption, this is not necessarily true, heavier storms could be accompanied by dry decades in the OESF. WE tested this hypothesis using a correlation test, which showed that erosion and storms only have a correlation Pearson coefficient of 0.35, which although positive, does not reveal a strong linear relationship between these two variables. Having said this, we nonetheless assumed that erosion and storms share the same intensity index r for a particular decade. This helped us simplify the model as the number of possible scenarios is greatly reduced with this assumption.

The Extreme Event Probability and Extra Erosion Realizations analysis was done for the 49 grid cells covering the OESF area. From now on however, our analysis will focus on the 4 grid cells that cover the Sol Duc River drainage road network, which is the actual area where the ARDM was tested. Applying formula (6.1) to every intensity-decade-road segment combination and then taking the average across grid cells yields the following results regarding the new full cost of reconstruction:

Intensity	1	2	3	4	5	6	7	8	9	10
Heavy	73870	72747	74463	83058	80773	84272	88809	86111	83523	83523
Moderate	57545	57513	58736	64084	62766	66091	68738	65695	63899	63899
Low	40717	41723	42673	45317	45028	48655	49876	46622	45607	45607

Table 6.4: Average full cost of road reconstruction for every period under each climate intensity

Table 6.4 shows a significant cost difference between the first 3 decades and the rest, where costs seem to stabilize until the end of the planning horizon. Two extra observations are that reconstructions costs reach their peak during the years 2070-2089 and that there is an important difference between the 3 climate intensities.

An even more important measure for evaluating the financial impact of climate change in infrastructure is the cost per length unit. It is a common forestry practice to measure this cost per length in USD/station, where one station is equivalent to 100 ft. Historically, the average cost per length value for the study area is 1850 USD/station. The next table shows how this value changes across decades and under different climate intensities:

Intensity	1	2	3	4	5	6	7	8	9	10
Heavy	2620	2641	2736	2892	2860	3002	3114	3032	2954	2954
Moderate	2111	2149	2216	2325	2310	2454	2544	2457	2404	2404
Low	1570	1629	1670	1733	1752	1914	1980	1891	1862	1862

Table 6.5: Average cost per station for every decade under each climate intensity.

We can observe similar results than in Table 6.4 regarding differences in decades and climate intensities. The peak is reached in the 7^{th} decade, where the average reconstruction cost per length is 68% higher than the historical value.

6.2 Scenario Generation

To build scenarios for the stochastic program, we used the New Road Reconstruction Cost Realizations. A scenario consists of a sequence of 10 climate intensities which then get translated into road reconstruction costs for every decade. As an example, sequence *Low-Low- Low-Moderate-Moderate-Moderate-Heavy-Heavy-Heavy-Heavy* represents a scenario where the climate intensity is *Low* in the first 3 decades, *Moderate* in decades 4-6 and *Heavy* through decades 7-10. Road reconstruction costs are then calculated accordingly to the considered scenario using formula (6.1).

It is important to emphasize that these climate intensities are only revealed in the **middle** of each decade, after the DM made harvesting and road reconstruction actions for that particular decade (which is assumed to occur at the **beginning** of the decade). This means that at the start of any decade, the DM is unaware of how the decade's climate intensity is going to be like, he/she only has information of how it has been in the previous decades. Another thing to have in mind is that because road reconstruction costs depend on future climate intensities (formula (6.1)), there is no one-to-one relationship between the decade's

climate intensity and its road reconstruction costs. The actual cost of reconstruction that a DM is going to end up paying is unknown at the time of repair. As it was explained in chapter 4.1, this cost is only revealed afterwards, and if a DM builds a low quality structure, the state charges him/her an extra fee later on for the extra maintenance costs by adjusting the his/her OF downwards (and upwards if it is the other way around).

This scenario structure has $3^{10} = 59.049$ possible scenarios (3 possible intensities in each one of the 10 decades), which can be too big in terms of computational effort. In order to reduce the number of scenarios, we assumed that decades inside their respective tridecade would share the same intensity: Decades 1, 2 and 3, which are part of the *First Tridecade*, will all have the same associated intensity r for a particular scenario s, and the same applies to the other two tridecades. Because there are only 3 tridecades in the planning horizon (*First Tridecade*= {Decades 1,2,3}, *Second Tridecade*= {Decades 4,5,6} and *Third Tridecade* = {Decades 7,8,9,10}), and decades inside a tridecade must have the same climate intensity, the scenario space is left with only 27 elements (3 possible intensities for each tridecade). Reducing the number of scenarios in such a way allowed us to show the benefits of a stochastic program without the computational burden of analyzing almost 60.000 scenarios.

The specific details and structure of these 27 scenarios and their interaction is explained in detail in the next chapter. We explain the structure of a *Scenario Tree* and how it was implemented to build the ARDM Stochastic Program, which shows a new adaptive strategy for harvesting and road reconstruction schedules under climate uncertainty.

Chapter 7

Stochastic Program

The 27 scenarios created in the previous chapter were used to model climate uncertainty in the ARDM. Although there are infinitely many possibilities for how future precipitations may turn out to be through this century, GCMs allow us to have an educated guess and a probability distribution for these potential scenarios. Using a finite number of scenarios that accurately represent the broad spectrum of plausible future precipitations over the OESF, we were able to build a stochastic programming framework to solve an optimization harvesting and road reconstruction problem over the Sol Duc River area. The specific details of this stochastic framework is best explained by a *Scenario Tree*, which is described next.

7.1 Scenario Tree:

To understand the concept of a scenario tree, let's introduce some notation first: Let $\mathcal{T}$ denote the set of periods in the planning horizon where $|\mathcal{T}| = \mathrm{T}$ is the number of periods ($\mathrm{T} = 10$ in this study). Let Ω be the set of possible scenarios, which in this case is 3^3=27 (three possible climate intensities in each one of the 3 tridecades). Now, as it was explained in the previous chapter, a scenario $\omega \in \Omega$ is a sequence of 10 decade climate intensities, which are then translated into road reconstruction costs using formula (6.1). A scenario is represented by a path from the root-node to a leaf-node in the scenario tree, where each node in the sequence represents the start of a particular decade where the DM has to make harvesting and road reconstruction decisions. On the other hand, edges coming out of the nodes represent the possible climate intensity for that node. We have to remember that the climate intensity is only revealed in the middle of the decade **after** the DM's harvesting and reconstruction actions made in the beginning of the decade, that is why it makes sense to model the climate intensity as the edge that leaves the node (this will become more clear with Fig 7.1). Finally, each scenario ω has an associated probability denoted by p^ω, with $\sum_{\omega\in\Omega} p^\omega = 1$.

For this project, it is assumed that transition probabilities from one climate intensity to another are constant, which means that going from a *Low* intensity decade to a *Low* intensity decade has the same probability as moving towards a *Moderate* or *Heavy* intensity decade. Although this may seem counter intuitive, this assumption comes from the fact that because

climate intensities were assumed to be constant during each tridecade, and tridecades are 30 year periods, climate can be considered temporally independent over such long periods of time. For this scenario tree, this means that if E_ω represents the sequence of edges forming scenario ω, then $p^\omega = \prod_{e \in E_\omega} \mathbb{P}(e)$, where $\mathbb{P}(e)$ represents the probability of edge e.

Now, let's denote by $\mathcal{N}^t$ the subset of parallel nodes belonging to period t such that $\mathcal{N} = \cup_{t \in \mathcal{T}} \mathcal{N}^t$ and $\mathcal{N}^t \cap \mathcal{N}^{t+1} = \emptyset$ for $t \in \mathcal{T} \setminus \{T\}$ (e.g. $\mathcal{N}^1$ is a singleton and $\mathcal{N}^2$ are 3 decision nodes after experiencing 3 different possible climate intensities in period 1). Let $\Omega(n)$ denote the set of scenarios that traverse node n. We have $\Omega(1) = \Omega$ and $\Omega(n) \cap \Omega(n') = \emptyset$ $\forall n \neq n' \wedge n,n' \in \mathcal{N}^t$. Let $\mathcal{I}_n$ denote the set of successor nodes to node n, for $n \in \mathcal{N}$ ($\mathcal{I}_n = \emptyset$ for $n \in \mathcal{N}^T$ (leaf-nodes)). Let's also define η as the set of nodes having more than one leaf-node as successor ($|\mathcal{I}_n \cap \mathcal{N}^T| > 1 \implies n \in \eta$). Consider X^ω the matrix of variables $\forall \omega \in \Omega$, and X^ω_n represent the vector of variables at node $n \in \eta$ under scenario $\omega \in \Omega$. Finally, let $\mathcal{Z}_n$ represent an auxiliary vector of variables at the node n and $f_\omega(\cdot)$ the linear function of the OF under scenario ω. With all this in mind, the stochastic program can be stated as follows:

$$max \sum_{\omega \in \Omega} p^\omega f_\omega(X^\omega) \tag{7.1}$$

$$\text{s.t. } X^\omega \in C^\omega \qquad \forall \omega \in \Omega \tag{7.2}$$

$$X^\omega_n = \mathcal{Z}_n \qquad \forall \omega \in \Omega(n), n \in \eta \tag{7.3}$$

Equation (7.1) maximizes the expected value from all scenarios, while equations (7.2) demand that the solution for a specific scenario respects that scenario's specific constraints (C^ω is the feasible set for scenario ω). Equations (7.3) on the other hand, impose non-anticipativity constraints, which require that the solution vectors of two scenarios should be the same in node n if the two scenarios are indistinguishable up to that node. Non-anticipativity constraints, or NACs assert that if two scenarios ω_i and ω_k are identical up to a certain period t, then the decisions made for scenarios ω_i and ω_k must also be identical up to period t. This means that under two different scenarios that are identical up to a period t, a DM should make the same decisions up to that period in both scenarios, because making different actions would be unrealistic and it would mean that DM is anticipating what is going to happen after t. Although NACs are a key and necessary element of multi-stage stochastic programming as they avoid unrealistic solutions, they usually make up a large constraint set making some problems much harder to solve.

The next figure shows the ARDM scenario tree representation for this study:

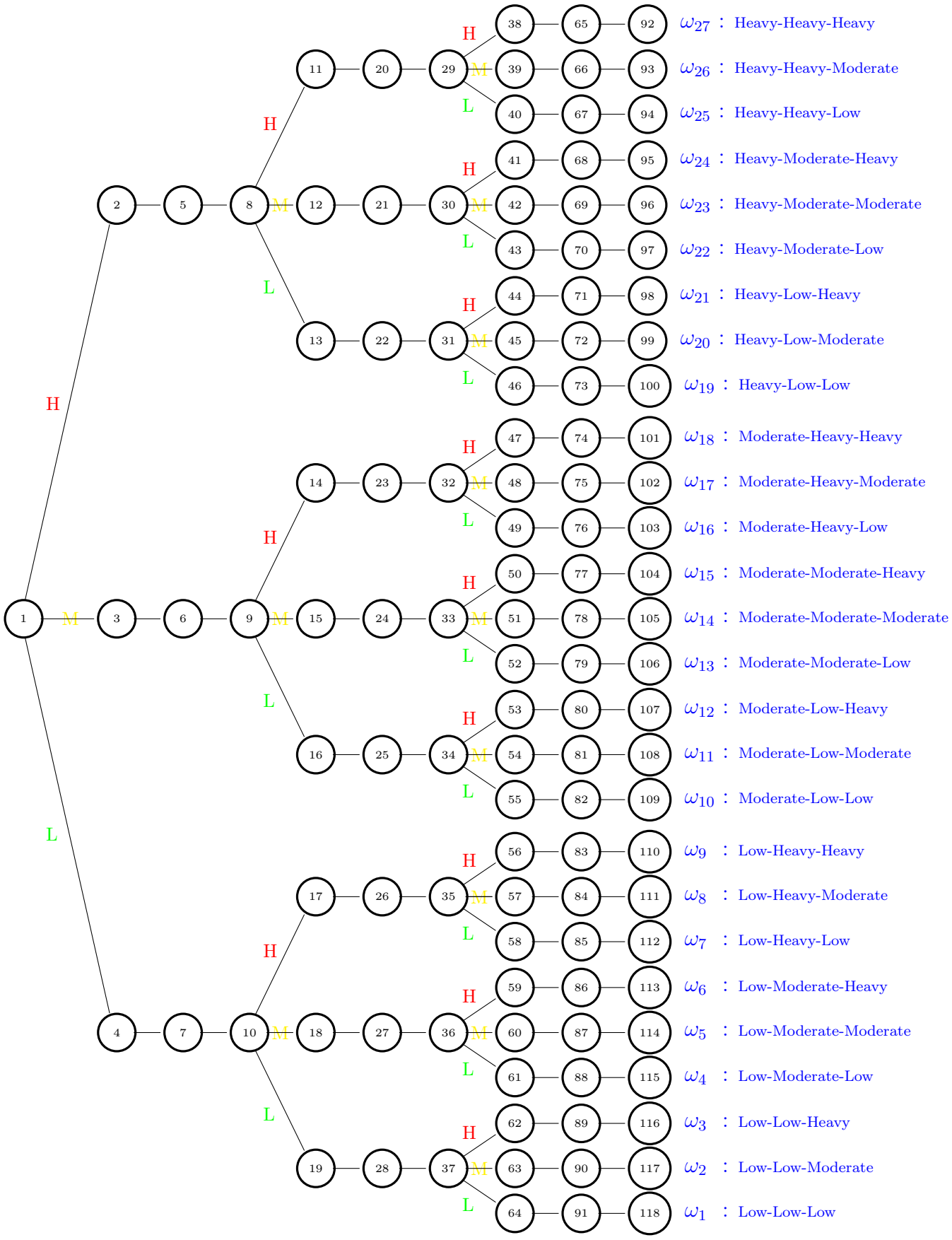

Figure 7.1: ARDM Scenario Tree representation.

This scenario tree consists of 118 nodes, 27 scenarios and 10 periods (T = $|\mathcal{T}| = 10$). Each node represents the start of a decade where the DM has to make a decision regarding harvest and road reconstructions. On the other hand, edges coming out of a node represent possible climate intensities of the source node under a specific scenario. When a node splits into 3 different leaves, each existing edge represents a different intensity path: *Low*, *Moderate* or *Heavy*, which are represented by the letters *L*, *M* and *H* respectively (Fig 7.1): For example, following the path from node 1 to node 97, we realize that scenario ω_{22} represents the {*H*, *H*, *H*, *M*, *M*, *M*, *L*, *L*, *L*} scenario, which is equivalent as saying that decades 1-3 have *Heavy* intensity climate, decades 4-6 have *Moderate* intensity climate and decades 7-10 have *Low* intensity climate. As it was previously mentioned, decades in the same tridecade have the same climate intensity, that is why nodes in period 2, 3, 5, 6, 8 and 9 have only one edge coming out of them. To have an idea of the scenario tree concepts previously defined, here are a couple of examples of how these concepts apply to the scenario tree in Fig. 7.1:

1. $\Omega(5) = \{\omega_1, \omega_2, \omega_3, \omega_4, \omega_5, \omega_6, \omega_7, \omega_8, \omega_9\}$, $\Omega(24) = \{\omega_{13}, \omega_{14}, \omega_{15}\}$, $\mathcal{N}^1 = \{1\}$, $\mathcal{N}^3 = \{5, 6, 7\}$, $\mathcal{I}_{35} = \{56, 57, 58\}, \mathcal{I}_{38} = \{37\}$ and $\eta = \mathcal{N} \setminus (\mathcal{N}^8 \cup \mathcal{N}^9 \cup \mathcal{N}^{10})$.
2. To exemplify NACs, we can see that for scenarios ω_{24}, ω_{25} and ω_{26}, climate intensities are identical up to the start of period 7 (node 30). This means that non-anticipativity constraints will force the solutions of periods 1-7 to be identical for ω_{24}, ω_{25} and ω_{26}, as the DM has identical information up to those periods.

7.2 Stochastic Program and Naïve Models

To measure the financial benefits of using the stochastic approach of the ARDM, we created 4 control models for comparison called the *Naïve Models* (NMs). NMs represent a naïve decision maker that doesn't take the uncertainty of future climate into consideration, and either believes there will be no climate change (which means that he/she assumes that future precipitation and storm events will behave exactly like the historical record) or gives probability 1 to a single scenario, meaning that it's in his/her belief that there is only one possible path for future climate change.

The most attractive naïve model to compare the ARDM to is the one were the DM completely ignores climate change. This comparison could potentially show the the financial risks of ignoring climate change in harvesting and road reconstruction planning, and serve as evidence for the non-scientific audience that is still skeptical about it. In the context of this work, a NM that doesn't take climate change into consideration believes in a 0% extra erosion for every decade, and a constant storm probability of 0.01 (which corresponds to the historical probability of a 100 year 24-hour event).

For this project, the ARDM was compared with 4 naïve models:

1. *Nocc_NM*: A DM that does not take climate change into consideration and projects an historical climate for the future.
2. *Low_NM*: A DM that believes in a *Low* intensity future. This DM is optimistic about future climate change and considers that extra erosion and storm probability will change in a *Low* intensity fashion for all 3 future tridecades.

3. *Mod_NM*: A more conservative DM that also uses climate projections for his/her decisions but assumes an average change. By taking an expected value for erosion and storms, this DM assumes a *Moderate* climate intensity for all 3 future tridecades.
4. *Heavy_NM*: A pessimistic DM that projects a *Heavy* climate intensity for all 3 future tridecades.

Contrary to the ARDM, the NMs believe in one possible intensity for the next 3 tridecades, and therefore concentrates the full probability distribution on it. One should expect that NMs perform worse than the ARDM, except maybe in scenarios that are very similar to the one that the naïve DM bases his/her harvesting and road reconstructions decisions on. This is because the ARDM gives a positive probability to every possible scenario, and even though it should outperform the NMs in most cases, a naïve DM could be lucky enough so that future climate behaves in a very similar way as he/she expected and based the harvesting and reconstruction decisions upon.

To compare the performance of the ARDM to the Naïve Models, their solutions were tested against all 27 scenarios to see how they performed under every possible future climate change trajectory[1]. The results of these model-scenario pairs are shown in the next **Results** chapter.

[1] we acknowledge that this is a simplifying assumption because there are infinite number of possible climate trajectories, but the 27 scenarios were designed to cover a wide range of them so that the results were as representative as possible.

Chapter 8

Results

8.1 Deterministic Model

The ARDM and the Naïve Models were applied to the Sol Duc River drainage area, which is made up of a total of 98 FMUs and 65 road segments, 53 of them having culvert infrastructure. The minimum rotation age was set to 40 years and the oldest age class in the initial inventory was set to 4 decades (parameters Z and P in Model II, respectively). Also, a 5% discount rate was applied to the model for two reasons: 1) When the EFCM was applied to the Upper ClearWater River landscape, the authors also applied a 5% discount rate, and so using that same value would make our results comparable. 2) After trying with different discount rates, we observed that as the discount rate was smaller, the ARDM's execution times grew in a non-linear way and it took more time to reach reasonable MIP gaps. A small discount rate was necessary in this study because future decades have a greater impact in the objective function as the value of this parameter gets smaller. With low discount rate values, two scenarios that only differ in the last decades can show significantly different solutions, unlike a situation where the last decades are not very relevant for the harvesting schedule and so these two scenarios end up with almost identical solutions. After analyzing the trade off between future decades relevance and execution times, we decided that the best decision was to set the discount rate to 5%. The ARDM and Naïve Models were solved using these parameters and tested against 27 climate scenarios, each scenario consisting of a sequence of climate intensities for each one of the 10 periods in the planning horizon (2010-2110), translated later into new road reconstruction costs (formula (6.1)).

Before comparing the performance between the ARDM and NMs, we decided to test a deterministic model under every scenario. This deterministic model has the same formulation as the ARDM and NMs but the only difference is that all the information of future road reconstruction costs is known in advance at the start of the planning horizon. Although this model is not very realistic, it serves as a benchmark (upper bound) for the other models and also to have an initial understanding of the problem and its solutions. Table 8.1 shows the solutions of this deterministic model under every scenario, showing the *Profit* (O.F. value), harvest and management profits (HMP), revenues (HMR), total costs (HMC), road reconstruction costs (RRC), number of FMUs accessed in the harvesting schedule ($\#FMUs$),

total volume harvested measured in MBF (*Volume*), number of roads segments reconstructed (*#Links)*, and total road length reconstruction (*#Stations*), measured in number of stations, which is equivalent to 100 ft.

Scenario	Profit	HMP	HMR	HMC	RRC	#FMUs	Volume	#Links	#Stations
Heavy-Heavy-Heavy	11699022	14177407	18552062	4374654	2478384	177	218752	130	4311
Heavy-Heavy-Mod	11728179	14178165	18554463	4376296	2449987	177	218437	128	4242
Heavy-Heavy-Low	11755538	14178165	18554463	4376296	2422627	177	218437	128	4242
Heavy-Mod-Heavy	11726146	14309290	18787785	4478493	2583144	179	221230	141	4614
Heavy-Mod-Mod	11750500	14308296	18793829	4485530	2557796	179	218814	138	4593
Heavy-Mod-Low	11774876	14308296	18795360	4487061	2533421	179	219315	138	4593
Heavy-Low-Heavy	11760471	14309290	18789316	4480024	2548818	179	221731	141	4614
Heavy-Low-Mod	11784649	14309290	18787785	4478493	2524640	179	221230	141	4614
Heavy-Low-Low	11808553	14315898	18809297	4493398	2507345	179	219014	141	4614
Mod-Heavy-Heavy	12211349	14331121	18806744	4475623	2119772	181	221896	156	4749
Mod-Heavy-Mod	12240687	14331121	18806744	4475623	2090434	181	221896	156	4749
Mod-Heavy-Low	12268050	14331121	18806744	4475623	2063071	181	221896	156	4749
Mod-Mod-Heavy	12232752	14347778	18845479	4497700	2115026	179	221849	141	4613
Mod-Mod-Mod	12257106	14346785	18851248	4504463	2089679	179	219341	138	4592
Mod-Mod-Low	12281482	14346785	18849991	4503206	2065304	179	218932	138	4592
Mod-Low-Heavy	12267077	14347778	18843948	4496169	2080702	179	221348	141	4613
Mod-Low-Mod	12291255	14347778	18843948	4496169	2056523	179	221348	141	4613
Mod-Low-Low	12315158	14354386	18864324	4509938	2039228	179	218761	141	4613
Low-Heavy-Heavy	12813721	14622188	19160791	4538604	1808467	183	223904	165	5095
Low-Heavy-Mod	12843059	14622188	19160791	4538604	1779129	183	223904	165	5095
Low-Heavy-Low	12870422	14622188	19160791	4538604	1751766	183	223904	165	5095
Low-Mod-Heavy	12813721	14622188	19160791	4538604	1808467	183	223904	165	5095
Low-Mod-Mod	12843059	14622188	19160791	4538604	1779130	183	223904	165	5095
Low-Mod-Low	12870422	14622188	19160791	4538604	1751766	183	223904	165	5095
Low-Low-Heavy	12816896	14634214	19198706	4564492	1817318	183	224056	167	5251
Low-Low-Mod	12843334	14630989	19183610	4552622	1787655	183	224944	166	5151
Low-Low-Low	12870422	14622188	19160791	4538604	1751766	183	223904	165	5095

Table 8.1: Deterministic model solutions under 27 climate intensity scenarios.

The deterministic model was solved to optimality under all scenarios for the same reason described in section 5.2: a gap could hide the profit difference in similar scenarios. Looking at the road reconstruction costs of the first 2 scenarios, *Heavy-Heavy-Heavy* and *Heavy-Heavy-Moderate*, the RRC difference is 28.397 USD, while the average OF (Profit) is 11.713.600 USD. This means that the RRC difference only represents a 0.24% of the average OF, and so, if the models were not solved to optimality then the MIP relative gap would hide the difference in the road reconstruction costs and both scenarios would probably have the exact same solution.

Continuing with the analysis of table 8.1, there are a number of interesting observations that can be drawn. On average, profits are approximately $12.3 million, total costs (harvesting and reconstruction costs) are $4.5 million and road reconstruction costs are $2 million. Costs represent 37% of the profits, road reconstruction costs represent 47% of the total costs and 17% of the profits. On the other hand, the OF values get higher as the scenarios get *less intense*, which makes sense because *more intense* scenarios represent higher road reconstruction costs. It should be pointed out that although there are pairs of scenarios where one is clearly more intense than the other (*Pareto* more intense), such as *Heavy-Heavy-Heavy* being more intense than *Heavy-Low-Low* and *Moderate-Moderate-Moderate* because the first one has a higher intensity in every tridecade, there are pairs of scenarios where this comparison

is not very clear. For example, scenario *a: Low-Heavy-Moderate* and *b: Low-Moderate-Heavy* are not comparable, because the first one is more intense in the second tridecade but less intense in the third. Even though we would expect that the solution for scenario a has a lower OF compared to scenario b because road reconstruction costs paid in tridecade 2 have a greater impact on the OF compared to the reconstructions made in tridecade 3 (because of the discount rate) and scenario a has a higher climate intensity in the second tridecade, the results show a different reality. Table 8.1 shows that scenario b has a lower OF than scenario a, even though we would expect the contrary. This shows that we should be careful in assuming certain results for pairs of scenarios that are not strictly comparable.

Looking at harvesting and maintenance revenues, costs and profits also increase for less intense scenarios, which can be explained by the fact that more FMUs were accessed in the solutions of these scenarios (although the difference is not very significant). One interesting observation is that less intense scenarios, scenarios where the first tridecade is of low intensity, make more road reconstructions and still have lower road reconstruction costs. Also, even though all scenarios are different between each other and were also solved to optimality, some of them have the exact same solution (this becomes clear by observing the *#FMUs*, *Volume*, *#Links* and *#Stations* columns of table 8.1: e.g scenarios *Mod-Heavy-Heavy*, *Mod-Heavy-Mod* and *Mod-Heavy-Low* have the same values for these columns). As it was explained earlier, this result is most likely explained by the fact that these scenarios are identical in the initial decades, and only differ in future decades that do not have an important impact in the OF (because of the discount rate). As a consequence, the schedule gives almost complete priority to the initial decades and the actions in future periods only adapt to this decisions.

After this initial understanding of the problem and the behaviour of its solutions, the next step was to analyze the solutions that come from applying the ARDM and NMs to every scenario. The objective was to see what conclusions drawn for the deterministic model (higher profits, harvest revenues, costs and lower road reconstruction costs for less intense scenarios) also apply to these two types of models and what new insights can we get from their solutions.

8.2 ARDM/Stochastic Model vs. Naïve Models

To test the benefits of the ARDM, a stochastic model that uses climate projections to optimize its harvesting and road reconstruction schedule, we compared it to the 4 naïve models described in section 7.2: *Low_NM*, *Mod_NM*, *Heavy_NM* and *Nocc_NM*. The next table shows the average computer runs made for each one of these models, which were solved using IBM ILOG CPLEX 64-bit 12.9.0 on an MSI GP62MVR 7RFX Server with an Intel(R) Core(TM) i7-7700HQ CPU @ 2.80GHz (eight processors) with 24 GB RAM and the Ubuntu 18.04.01 Server 64-bit operating system. It includes the computational run times of the ARDM and **all** the other naïve models: Although in this project we only compared the ARDM to the 4 naïve model just mentioned, this table also shows all the 28 possible naïve models, which are 28 DMs believing in only one (out of the 28 scenarios, considering the no-climate-change scenario) possible scenario for the future.

Model	Time (minutes)
ARDM	440
Nocc_NM	2.73
Heavy-Heavy-Heavy	9.96
Heavy-Heavy-Mod	7.56
Heavy-Heavy-Low	3.30
Heavy-Mod-Heavy	6.47
Heavy-Mod-Mod	3.33
Heavy-Mod-Low	4.00
Heavy-Low-Heavy	6.8
Heavy-Low-Mod	3.75
Heavy-Low-Low	3.5
Mod-Heavy-Heavy	6.2
Mod-Heavy-Mod	5.30
Mod-Heavy-Low	3.51
Mod-Mod-Heavy	7.65
Mod-Mod-Mod	4.78
Mod-Mod-Low	2.98
Mod-Low-Heavy	7.42
Mod-Low-Mod	3.93
Mod-Low-Low	3.88
Low-Heavy-Heavy	3.21
Low-Heavy-Mod	4.28
Low-Heavy-Low	1.85
Low-Mod-Heavy	7.1
Low-Mod-Mod	3.2
Low-Mod-Low	2.48
Low-Low-Heavy	12.77
Low-Low-Mod	2.15
Low-Low-Low	2.03

Table 8.2: Average computational time runs for each model. The models highlighted in light blue are the ones used for this project, where the 'Heavy-Heavy-Heavy' row represents the *Heavy_NM*, the 'Mod-Mod-Mod' row represents the *Mod_NM* and the 'Low-Low-Low' row represents the *Low_NM*.

One thing to notice is that each model has only one computational time, not one for each of the 27 scenarios under which they were tested. In the case of he ARDM, this is because the stochastic model is solved simultaneously for all the scenarios taking into consideration non-anticipativity constraints. In the case of the naïve models, this is because their solution is **evaluated** under each scenario, but the solution is exactly the same. The decisions of a naïve DM are not affected by the climate he/she sees during the planning horizon, and so testing the model in each scenario is equivalent as taking the unique solution and evaluating it under all the particular scenarios' new road reconstruction costs.

The ARDM was solved to a 0.3% MIP gap and all the other models were solved to optimality. The ARDM takes on average 7.3 hours to reach this gap, which is explained by the large scenario structure and its NACs constraints that drastically increase the size of the problem. Regarding the naïve models, their average computational times range from 2 to 13 minutes with an average of 4.86 minutes, but there is not a clear pattern of their behaviour regarding the different intensities.

The next table shows the OF (Profit) of the 5 models evaluated in every scenario:

Scenario	ARDM	Low_NM	Mod_NM	Heavy_NM	Nocc_NM
Heavy-Heavy-Heavy	11684335	11517515	11689578	11699022	11671239
Heavy-Heavy-Mod	11711097	11546853	11715664	11728158	11697609
Heavy-Heavy-Low	11735710	11574216	11740040	11755339	11722225
Heavy-Mod-Heavy	11697504	11517515	11721306	11699022	11688602
Heavy-Mod-Mod	11726413	11546853	11747392	11728158	11714972
Heavy-Mod-Low	11753536	11574216	11771768	11755339	11739588
Heavy-Low-Heavy	11744850	11517515	11753499	11699022	11705898
Heavy-Low-Mod	11770790	11546853	11779585	11728158	11732268
Heavy-Low-Low	11795166	11574216	11803961	11755339	11756884
Mod-Heavy-Heavy	12209139	12153940	12199292	12198934	12209139
Mod-Heavy-Mod	12235391	12183278	12225378	12228070	12235509
Mod-Heavy-Low	12260032	12210641	12249754	12255251	12260125
Mod-Mod-Heavy	12226502	12153940	12231020	12198934	12226502
Mod-Mod-Mod	12252177	12183278	12257106	12228070	12252872
Mod-Mod-Low	12277141	12210641	12281482	12255251	12277488
Mod-Low-Heavy	12242450	12153940	12263213	12198934	12243798
Mod-Low-Mod	12268820	12183278	12289299	12228070	12270168
Mod-Low-Low	12293343	12210641	12313675	12255251	12294784
Low-Heavy-Heavy	12808273	12813721	12728356	12717756	12767643
Low-Heavy-Mod	12837392	12843059	12754442	12746892	12794013
Low-Heavy-Low	12865431	12870422	12778818	12774073	12818629
Low-Mod-Heavy	12799678	12813721	12760084	12717756	12785006
Low-Mod-Mod	12837720	12843059	12786170	12746892	12811376
Low-Mod-Low	12865777	12870422	12810546	12774073	12835992
Low-Low-Heavy	12807728	12813721	12792277	12717756	12802302
Low-Low-Mod	12830809	12843059	12818363	12746892	12828672
Low-Low-Low	12864430	12870422	12842739	12774073	12853288

Table 8.3: Profit comparison of 5 models. Values in green represent scenarios in which the ARDM outperforms the corresponding NM, while values in red represent the contrary.

The first observation is that, the same as in the deterministic models, the OF increases as scenarios get less intense. On the other hand, going from highest to lowest in terms of profit, the ARDM has a weighted average (weights given by the different scenario probabilities) profit of \$12.268 million, *Mod_NM* has an average profit of \$12.261 million, *Nocc_NM* an average of \$12.258 million, *Heavy_NM* has an average of \$12.232 million, and finally, *Low_NM* has an average of \$12.189 million.

Before continuing with the analysis, it is important to reflect on the fact that the previous result does not show a very big difference between models in terms of profit. The biggest difference is between the ARDM and the *Low_NM* models, with a difference of approximately \$80 thousand that only represents a 0.7% improvement. With this in mind, one could be tempted into concluding that the benefits of using a stochastic model are irrelevant, but

there are 2 reason why this is incorrect. First, as it was mentioned earlier, the final area of study selected for this work is very small compared to the original, and in a real life harvest schedule, it would only represent a small fraction of the complete forest. Compared to the UCW, the harvesting area of this study is 6 times smaller and 56 times smaller than the OESF. Although we can not simply scale up the cash flows by acres because they are greatly dependent on factors such as maturity of timber and age class distribution, revenues and costs generally increase with the size of forest. If the ARDM was applied to this big areas, and we assumed a linear scaling of cash flows, the $80 thousand difference captured by the ARDM would be translated into $480 thousand and $4.5 million for the UCW and OESF, respectively. Event though this is just an approximation, these new figures are not insignificant at all and show a great potential for this stochastic model.

A second reason is that the costs in this model only consider harvesting, management and road reconstruction costs, and do not consider the fixed cost of buying/renting the land. On DNR land for example, the right to harvest forest stands is given competitively via auctions where the highest bidders are awarded contracts to cut and haul timber, where the bare land value is approximately $2500 per acre. Given that this renting cost was not included in the model's OF, this means that the total profits for the foresters are much lower than what is shown in table 8.3, and therefore the $80 thousand difference represents more than a 0.7% improvement. Assuming a cost of $2500 per acre, the bare land value of this study area would be $10.5 million (4200 acres), and the new weighted average profits for every model would be: $1.768 million for the ARDM, $1.762 million for the *Mod_NM*, $1.758 million for the *Nocc_NM*, $1.732 million for the *Heavy_NM* and $1.688 million for the *Low_NM*. The biggest profit difference is also between the ARDM and *Low_NM*, with the same value of $80 thousand, but now represent a 4.7% improvement.

Going deeper into the 5 models' solution analysis, the next figure shows how the profit (not considering land renting costs) difference between the ARDM and NMs changes for different scenarios:

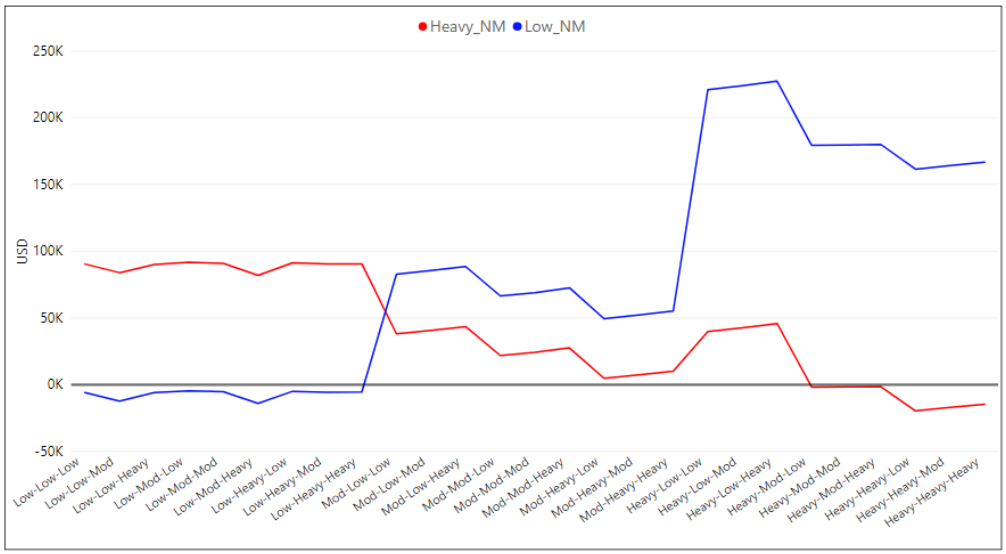

Figure 8.1: ARDM vs. *Heavy_NM* and *Low_NM*: Profit difference (ARDM *minus* NM) under the 27 scenarios.

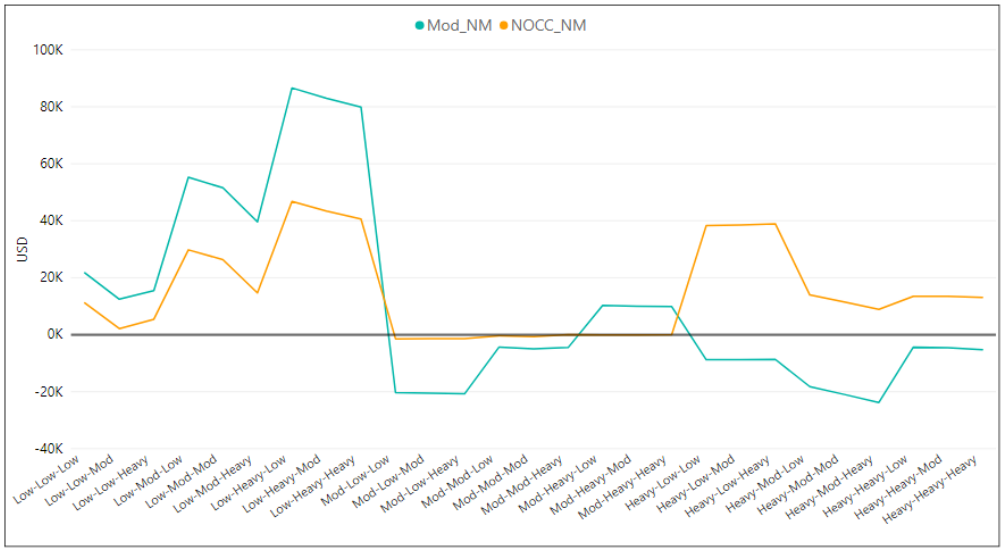

Figure 8.2: ARDM vs. *Mod_NM* and *Nocc_NM*: Profit difference (ARDM *minus* NM) under the 27 scenarios.

Figure 8.1 shows that when the DM has a *Low Naïve* approach, it outperforms the ARDM in the first 9 scenarios, where the intensity in the first tridecade is *Low*. Although the average difference is not very big ($7.152 USD), it makes sense that the naïve model performs better than the ARDM when they are evaluated in these scenarios because the naïve DM puts all the probability in the *Low-Low-Low* scenario, which is identical to these scenarios in the first tridecade (the decades that have the highest impact in the OF). As the scenarios move "further" away from *Low-Low-Low*, the benefits of using a stochastic approach get bigger, with a maximum difference of $223 thousand compared to the NM. In the case of the *Heavy_NM* model also shown in figure 8.2, the conclusions are exactly the opposite: The NM outperforms the ARDM only in the 6 most intense scenarios, with an average difference of $9 thousand. As scenarios move "further" away from the *Heavy-Heavy-Heavy* scenario, the ARDM performs better than the NM, with a maximum difference of $91.7 thousand.

On the other hand, Figure 8.2 also shows very interesting results: The "No climate change" model is only better (or equal) than the ARDM model in scenarios where the first tridecade has *Moderate* intensity, although the benefits are very small (600 USD on average). On the other scenarios, the ARDM outperforms the *Nocc_NM* with a maximum profit difference of $46 thousand. The analysis of the profit difference between the ARDM and *Mod_NM* show somewhat different results than the ones observed in the other 3 naïve models. The naïve model in this case outperforms the ARDM in more than 50% of the total scenarios (15 vs. 12). The *Mod_NM* has better solutions than the ARDM in all the scenarios that start with a *Heavy* intensity tridecade, and in most of the scenarios that start with a *Moderate* intensity tridecade. In contrast, the stochastic model has a higher OF in scenarios with low intensity climate for the first tridecade, with a maximum difference of $86 thousand. It seems that the conservative naïve model that assumes a constant moderate intensity is the best naïve alternative to the stochastic model.

The next table shows a summary of the performance of the ARDM versus the 4 naïve models, showing the number of scenarios where the ARDM has a higher/lower OF than each NM (#<ARDM and #>ARDM respectively), the worst case scenario loss of each NM compared to the ARDM (*Worst Case*), the best case scenario benefit (*Best Case*) , and the weighted average profit benefit ($\overline{\text{Profit Benefit}}$) of this new stochastic model against all the other NMs:

Model	$\overline{\text{Profit Benefit}}$	#<ARDM	#>ARDM	Worst Case	Best Case
Heavy_NM	35.728	21	6	-91.704	19.629
Mod_NM	6.404	12	15	-86.613	23.802
Low_NM	79.414	18	9	-227.335	14.043
Nocc_NM	10.469	20	7	-46.802	1441

Table 8.4: Solutions comparison between ARDM and NMs.

The naïve model that minimizes the weighted average profit (calculated across all scenarios) difference with the stochastic model is the *Mod_NM*, with a value of 6.404 USD, followed by the *Nocc_NM*. This shows that even though the *Mod_NM* has a better win rate over the ARDM, this stochastic model still yields better results in terms of average profit. The model that does worse in this metric is the *Low_NM*, followed by the *Heavy_NM*. The most likely reason for this results is the fact that the *Mod_NM* is the one that best approximates the expected climate intensity for future periods, followed by the "no climate change" approach. The *Low* approach is too naive with regards to the future and underestimates the future reconstruction costs, that is why it is the worst performing model. On the other hand, the *Heavy* intensity approach is the second worst, probably because the DM's decisions in this model are too cautious and inefficient.

With this results in mind, a DM that wants to compete with the ARDM to minimize the OF difference across scenarios should probably make his/her decisions assuming a moderate future climate change for all the planning horizon. On the other hand, a more risk averse forester could try to minimize the worst case scenario. For this matter, the results show that a "no climate change" model is the best approach that this DM can take, even better than the *Mod_NM* and the *Heavy_NM* (with the downside of having the lowest "Best Case" scenario). The *Nocc_NM* and the *Heavy_NM* are the models that have the lowest win rate against the ARDM in terms of scenarios with better solutions, while the moderate approach yields the best results in this metric.

8.2.1 Schedule comparison: ARDM vs. NMs

Besides the profit difference between models, it is also interesting to analyze how the solutions differ regarding harvesting and road reconstruction actions. To motivate this analysis, let's observe the differences in timber extraction and road reconstruction schedules between the best performing naïve model, *Mod_NM*, and the stochastic model, in the *Low-Heavy-Low* scenario, where we find that the OF difference is the biggest:

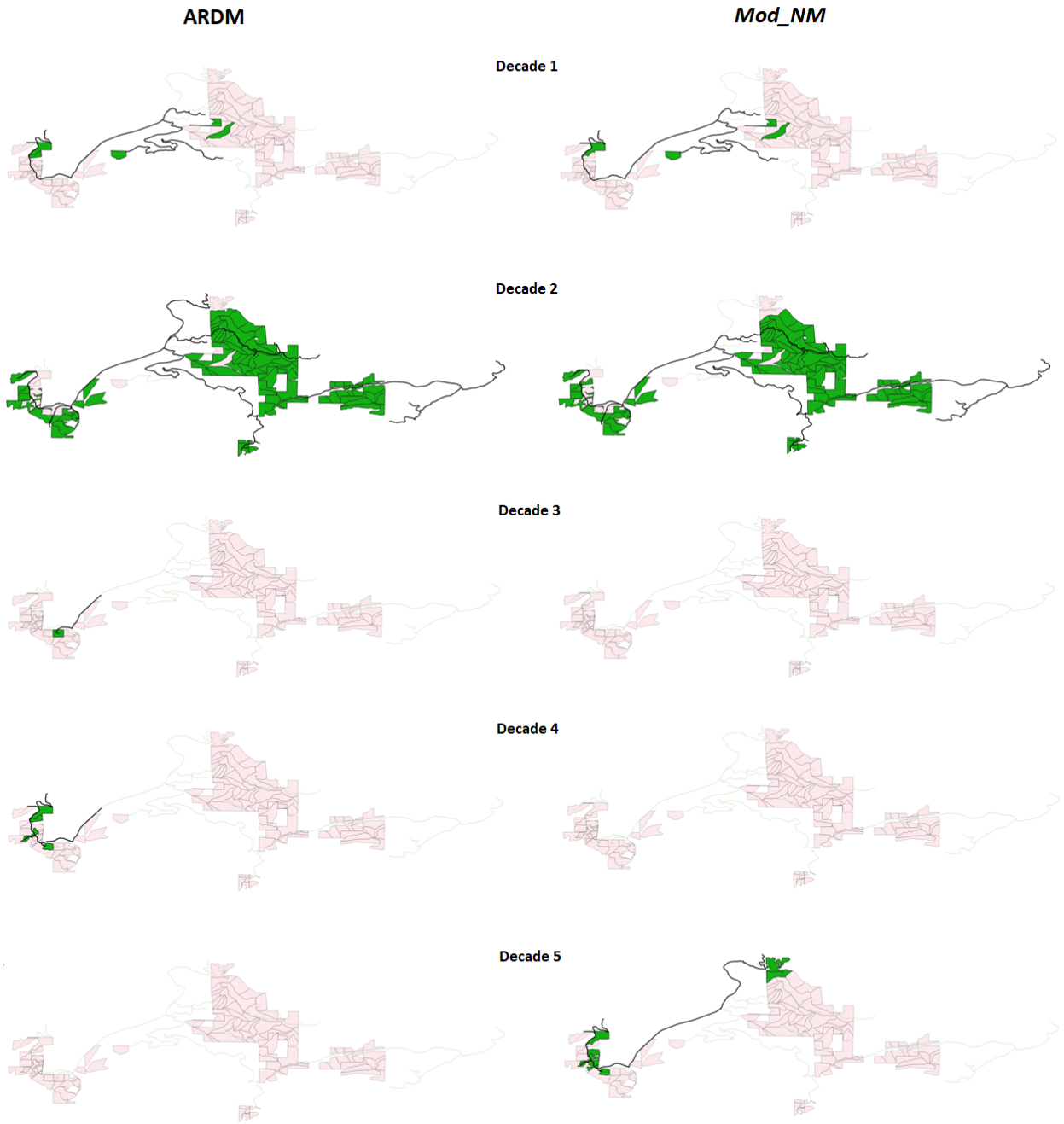

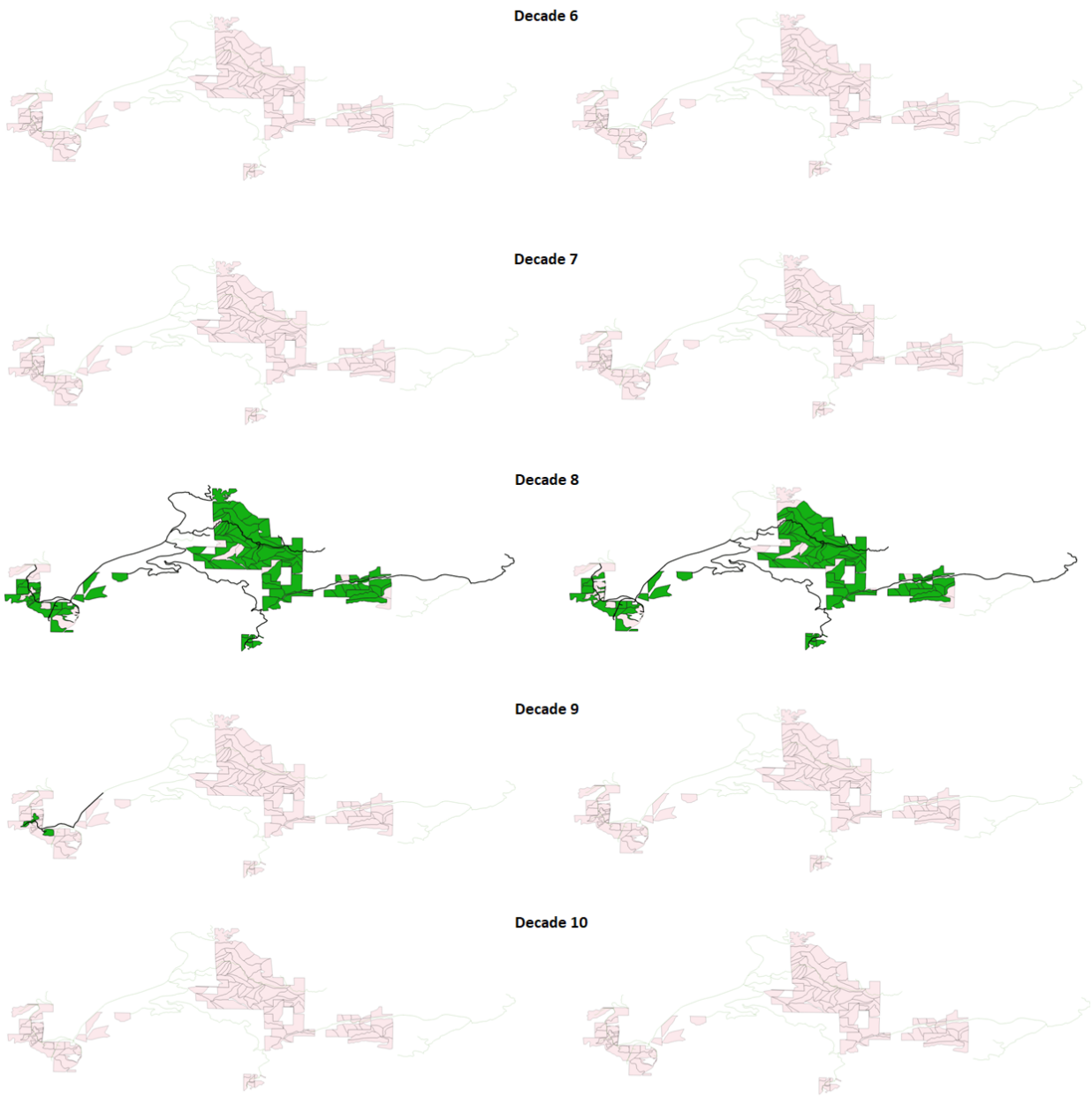

Figure 8.3: ARDM (left) vs. *Mod_NM* (right): Harvest and road reconstruction actions under the *Low-Heavy-Low* scenario. Green FMU's are the ones accessed during that period, while black road segments are the ones that are reconstructed.

These actions can be summarised in the next table, where *HMR* represents the *Harvest & Management Revenues*, *HMC* is Harvest & Management Costs, *HMP* is Harvest & Management Profits, *Area* is the total area of the FMUs harvested (measured in acres), *Total Volume* is the harvested timber volume (measured in MBF), *RRC* is Road Reconstruction Costs, the *Tier1 RRC* and *Tier2 RRC* fields represent the road reconstruction costs at cost tier 1 and 2 respectively, and *Total Length* is the length of the reconstructed network in that particular period (measured in number of stations (100 ft.)):

Field\Decade	1		2		3		4			5			6		7		8		9			10	
Profit	1811859	1740276	23062623	23104195	19241	0	184125	0	0	133652	0	0	0	0	12140107	11140243	37194	0	0	0
HMR	2757956	2667639	33043025	32785726	145539	0	873202	0	0	2745414	0	0	0	0	28908682	26552859	431395	0	0	0
HMC	389011	370268	7819086	776739	66864	0	349131	0	0	1261899	0	0	0	0	14195327	13112788	285530	0	0	0
HMP	2368955	2297372	25223939	25020986	78675	0	524071	0	0	1483515	0	0	0	0	14713355	13440070	145865	0	0	0
#FMUs	5	4	87	87	1	0	4	0	0	7	0	0	0	0	84	81	2	0	0	0
Area	256	232	4170	4118	39	0	159	0	0	382	0	0	0	0	4071	3849	63	0	0	0
Total Volume	5523	5245	113318	112571	466	0	3249	0	0	10006	0	0	0	0	99847	91110	1382	0	0	0
RRC	557096	557096	2161316	1916790	59434	0	339947	0	0	1349863	0	0	0	0	2573248	2299866	108671	0	0	0
Tier1 RRC	233842	233842	339398	339398	56410	0	37801	0	0	0	0	0	0	0	0	0	83053	0	0	0
Tier2 RRC	323254	323254	1821919	1577393	3024	0	302145	0	0	1349863	0	0	0	0	2573248	2299866	25618	0	0	0
#Reconstr.	20	20	57	50	9	0	12	0	0	21	0	0	0	0	55	47	10	0	0	0
#Tier1 Reconstr	13	13	17	17	8	0	5	0	0	0	0	0	0	0	0	0	7	0	0	0
#Tier2 Reconstr	7	7	40	33	1	0	7	0	0	21	0	0	0	0	55	47	3	0	0	0
Total Length	778	778	1854	1675	100	0	277	0	0	562	0	0	0	0	1762	1577	156	0	0	0

Table 8.5: Model comparison for every decade: ARDM (white) vs. *Mod_NM* (light blue)

There are a couple of interesting things to notice in the previous figure and table:

1. Both models have very similar actions for the first and second decade.
2. Both models have decades in which no harvesting or road reconstruction is performed. There are two main reasons for this: First, the even flow constraints were eliminated from the model, which allows consecutive periods to have drastically different volumes of timber harvested. A DM may decide to harvest all FMUs in one decade and nothing the next. Second, trees have a rotation age of 40 years, and so the same FMUs cannot be accessed over and over again. After a big harvest decade, it is better to hold extraction for a couple of years before reconstructing road segments and re-accessing the FMUs.
3. The "Big Harvests" occur in the same decades (2^{nd} and 8^{th}), and they represent almost the complete harvest volume of the planning horizon. For the ARDM model, 95% of the total volume is harvested in period 2 and 8, and for the *Mod_NM*, 93% is harvested in those periods.
4. Some decades show activity for one model and no activity at all for the other one. Having said this, periods where this occurs (3, 4, 5 and 9) do not show many reconstruction or harvest actions done on behalf of the active model.
5. The ARDM model makes more reconstructions (163 vs. 138) and accesses more FMUs (183 vs. 179) during the planning horizon, which results in 4853 extra MBF. harvested timber and an extra total length reconstruction of 10 km.

Although it would be interesting to do this analysis for all naïve models under every scenario, it is not practical because the combinations are too many (108 combinations: 27 scenarios for the 4 naïve models). We can replace this by observing the actions of every naïve model, which do not depend on the scenario (that is why they are called naïve DMs, they do the same actions under every scenario, what changes is the cost of road reconstructions) and compare this to the weighted average solution of the ARDM model across all scenarios. This will show the general differences in the actions that these 5 models take:

Feature	ARDM	*Heavy_NM*	*Moderate_NM*	*Low_NM*	*Nocc_NM*
#FMUs	181	177	179	183	182
Area (acres)	8646	8432	8581	8759	8682
Total Volume (MBF.)	220869	218752	219843	223904	222219
#Reconstr.	155	130	138	165	157
#Tier1 Reconstr.	47	32	30	52	50
#Tier2 Reconstr.	108	98	108	113	107
Total Length (#stations)	4808	4311	4592	5095	4848

Table 8.6: Schedule comparison between all models

The first thing to notice is that the *Low_NM* is the most active model, both in terms of harvesting and road reconstruction decisions, followed by the ARDM and *Nocc_NM* models. The *Low_NM* has the highest percentage of road reconstructions made at cost tier 1 (31.5%), followed closely by the ARDM model (30%), and also has the highest volume harvested compared to other models (although it is only 1.3% higher than the average). Although the ARDM model has similar results than the *Low_NM* at a global scale, its results in terms of profit are much better because the timing is better. Because the *Low_NM* model is very optimistic about the future, the DM takes unnecessary actions and also with bad timing. Among all models, the *Heavy_NM* model is the less active, which makes sense because this DM is very cautious about future climate change and prefers to avoid unnecessary reconstructions, which translates into a downside in terms of profit.

Table 8.4 showed that the *Mod_NM* model outperforms the stochastic model in more than 50% of the scenarios and has the lowest weighted average profit difference compared to the ARDM. Nonetheless, the ARDM is, on a average, a better performing model. Table 8.6 shows that the ARDM has higher activity than the *Moderate_NM* in every aspect, and it appears than having higher harvesting and reconstruction actions performed at the right timing (thanks to the information regarding climate projections) gives the necessary advantage for this model to produce more profitable schedules. Although the results differ across scenarios, the ARDM has a conclusive better performance than the other naïve models, probably thanks to its preemptive and data driven approach.

Chapter 9

Conclusions

Climate change will have a progressively higher impact on the world as we move through this century. Global air temperatures will rise, there will be an increasing risk of fire, and precipitation patterns will get more severe. The data shows that we can specifically expect a more vigorous hydrological cycle in terms of annual precipitation and bigger, more frequent rain storm events. Among all the consequences this will have for foresters, the ones analyzed in this study were the accelerated road decay as a consequence of higher erosion rates and the increasing probability of storm events that have the potential of altering channel width and thus destroy culvert infrastructure.

Using a set of 12 GCMs from the Climate Model Inter-comparison Project, we were able to build these two precipitation effects for the next century and translate them into a new stochastic road reconstruction cost structure. Using these new cost parameters and building on the EFCM, we constructed the ARDM, the first formulation for optimal adaptation of forest roads maintenance and uncertain road access to timber resources due to climate change. This model was applied to the Sol Duc River drainage area, a 150 km^2 forest land-base located in the Olympic Experimental State Forest in Washington State with a 63.5 km. road network.

To test the benefits of using the ARDM under a climate uncertain future, we compared this model to 4 naïve approaches, where each of these formulations models a decision maker that either does not have information of future precipitation projections, or believes in one single climate scenario. Unlike the ARDM, which adapts its strategy throughout the planning horizon, these "stubborn" DMs stick to their initial schedule and continue with their harvesting and road reconstruction decisions ignoring precipitation patters along the decades.

The stochastic and naïve models were tested against 27 climate scenarios that well represent the range of potential future climate trajectories. It was interesting to see that some naïve models outperformed the ARDM in particular scenarios, usually the ones that most closely resembled that particular DM's naïve approach. Although the stochastic model clearly was a more profitable approach compared to the other models, the *Mod_NM*, which represents a forester who believes in an average climate intensity (expected value from the GCM's projections) for the whole century, was the best candidate at competing with the ARDM in terms of profit.

The ARDM has a $33 thousand dollar average profit difference compared to the naïve models, and outperforms the *Low Naïve model* by $80 thousand. When the costs of renting the land are considered, we see an average profit improvement of 2% compared to the naïve models (4.7% compared to the *Low Naïve model*). Although the overall profit improvement may seem small, it can be explained by several factors like the ones that were discussed during this study. First, the use of 5 % discount rates over a large time span significantly attenuates any savings that accrue more than 30 years into the future. Although smaller discount rates were evaluated, their impact in the computational run times and MIP gap was significant. Considering the fact that getting close to optimal solutions in a reasonable time was very important, a 5% discount rate value was finally deemed to be the best option. Second, the area of study was too small, 6 times smaller than the area where the EFCM was applied (Upper ClearWater). In addition to the fact that profits increase with the size of the forest, having a more complex road network would also allow the ARDM to show its preemptive and adaptive potential by finding cheaper hauling routes. When there are too few options to choose from (65 road segments in this study), the ARDM is not allowed to show its full potential.

We are confident that the benefits of the ARDM would drastically improve if it was applied to a bigger area with a lower discount rate and considering a wider range of climate intensities. To do this, we would have to change the ARDM non-anticipativity constraints (responsible for the huge size of the problem and its inefficiency) by another algorithm such as the Progressive Hedging approach (PH), which was used by Veliz et al. (2015) and many others in the past years. A PH algorithm solves each scenario independently and only then uses a convergence heuristic to force non-anticipativity on nodes and pair of scenarios that require it. It is a much better solution for stochastic problems when the size of the instance and number of scenarios increases, and it would allow the ARDM to be applied in larger areas with a much bigger set of scenarios and more complex road network.

9.1 Final Thoughts

In these last decades, we have seen how climate change has produced increasingly negative effects to our planet. Based on the increasing melting of the North Pole, more frequent and intense hurricanes in the North Atlantic and devastating fires affecting countries such as Brazil, Australia and the US, it is clear that these serious effects of our changing climate have to be dealt with. It is important that we take decisive actions to reduce the emissions of greenhouse effects and take a step towards a more sustainable economy with a greater consideration for wildlife and nature. In the field of forestry, scientists have already started studying the effects of climate change and the use of integrated managing to increase both revenue production and ecological sustainability (e.g. DNR in the OESF). Building on the work of many other researchers, the ARDM is a new formulation that aims to improve this same integrated managing approach by considering the effects of precipitation on road networks. Although there is a long way ahead and some modifications have to be done in order to create a more robust model, this study shows the ARDM's great potential and its ability to include an important effect of climate change in its adaptive formulation.

Appendix

A: Final Model

$$\max \quad \sum_{l=1}^{|T|} \sum_{k=-P}^{l-Z} \sum_{m} A_m \rho_{m,k,l} W_{m,k,l} - \sum_{i,j,t} \phi_j \alpha_i s_{i,t}^j 1.05^{10(1-t)} \tag{9.1a}$$

$$\text{s.t.} \quad \sum_{j} s_{i,t}^j \leq 1 \qquad \forall i \in I, t \in T, \tag{9.1b}$$

$$\sum_{k=1}^{J} s_{i,t-j}^k \geq s_{i,t}^j \qquad \forall i \in I, t \in T, j \in J, \tag{9.1c}$$

$$\sum_{j \in j_{in}} F_{(p,q)} + \sum_{m \in U_j} x_{m,t} = \sum_{k \in j_{out}} F_{(q,k),t} \qquad \forall j \in V, t \in T, \tag{9.1d}$$

$$\sum_{p \in V_\tau} F_{(p,\tau),t} = \sum_{m} x_{m,t} \qquad \forall t \in T, \tag{9.1e}$$

$$N \sum_{k} s_{(i,j),t}^k \geq F_{(p,q),t} \qquad \forall (p, q \neq \tau), t \in T, \tag{9.1f}$$

$$N_{m,k} + \sum_{l=1}^{|T|} W_{m,k,l} = a_{m,k}, \qquad \forall m \in M, k = -P, ..., 0, \tag{9.1g}$$

$$N_{m,k} + \sum_{l=k+Z}^{|T|} W_{m,k,l} = \sum_{t=-P}^{k-Z} W_{m,t,k}, \qquad \forall m \in M, k = 1, ..., |T|, \tag{9.1h}$$

$$\sum_{m} \sum_{k=-P}^{l-Z} v_{m,k,l} W_{m,k,l} = H_l, \qquad \forall l = 1, ..., |T|, \tag{9.1i}$$

$$\sum_{k=-M}^{t-Z} W_{m,k,t} \geq H_{min} x_{m,t} \qquad \forall m \in M, t \in T, \tag{9.1j}$$

$$\sum_{k=-M}^{t-Z} W_{m,k,t} \leq H_{max} x_{m,t} \qquad \forall m \in M, t \in T, \tag{9.1k}$$

$$1.25 H_t \geq H_{t+1} \qquad \forall t = 1, ..., |T| - 1, \tag{9.1l}$$

$$0.75 H_t \leq H_{t+1} \qquad \forall t = 1, ..., |T| - 1, \tag{9.1m}$$

$$\sum_{m} \sum_{t=-P}^{|T|} Age_{t,|T|} N_{m,t} A_m \geq \sum_{m} \sum_{t=-P}^{-1} Age_{t,1} a_{m,t} A_m \tag{9.1n}$$

B: CDF

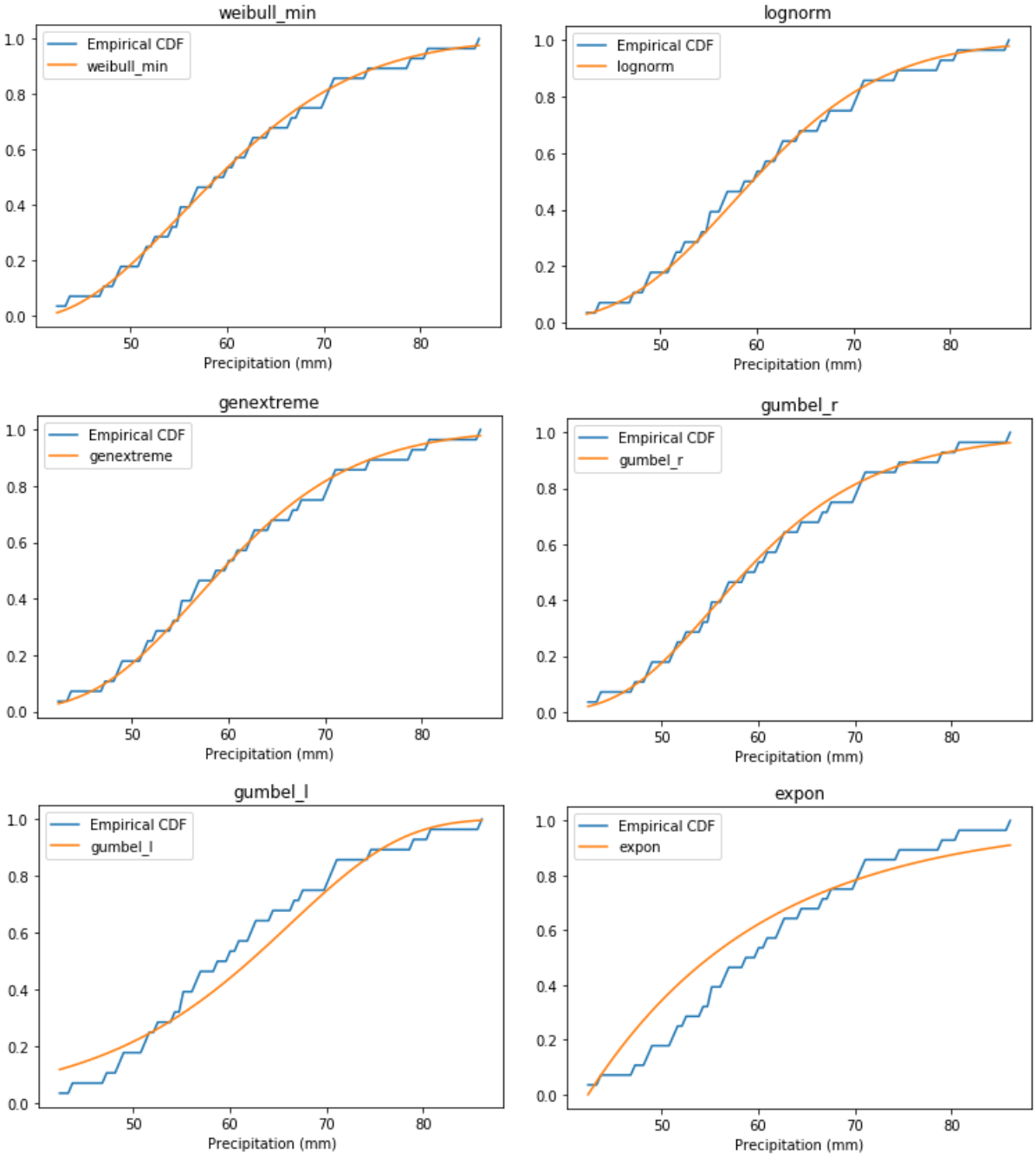

Figure 9.1: Empirical vs Theoretical CDF of 6 distributions.

C: QQ-plot

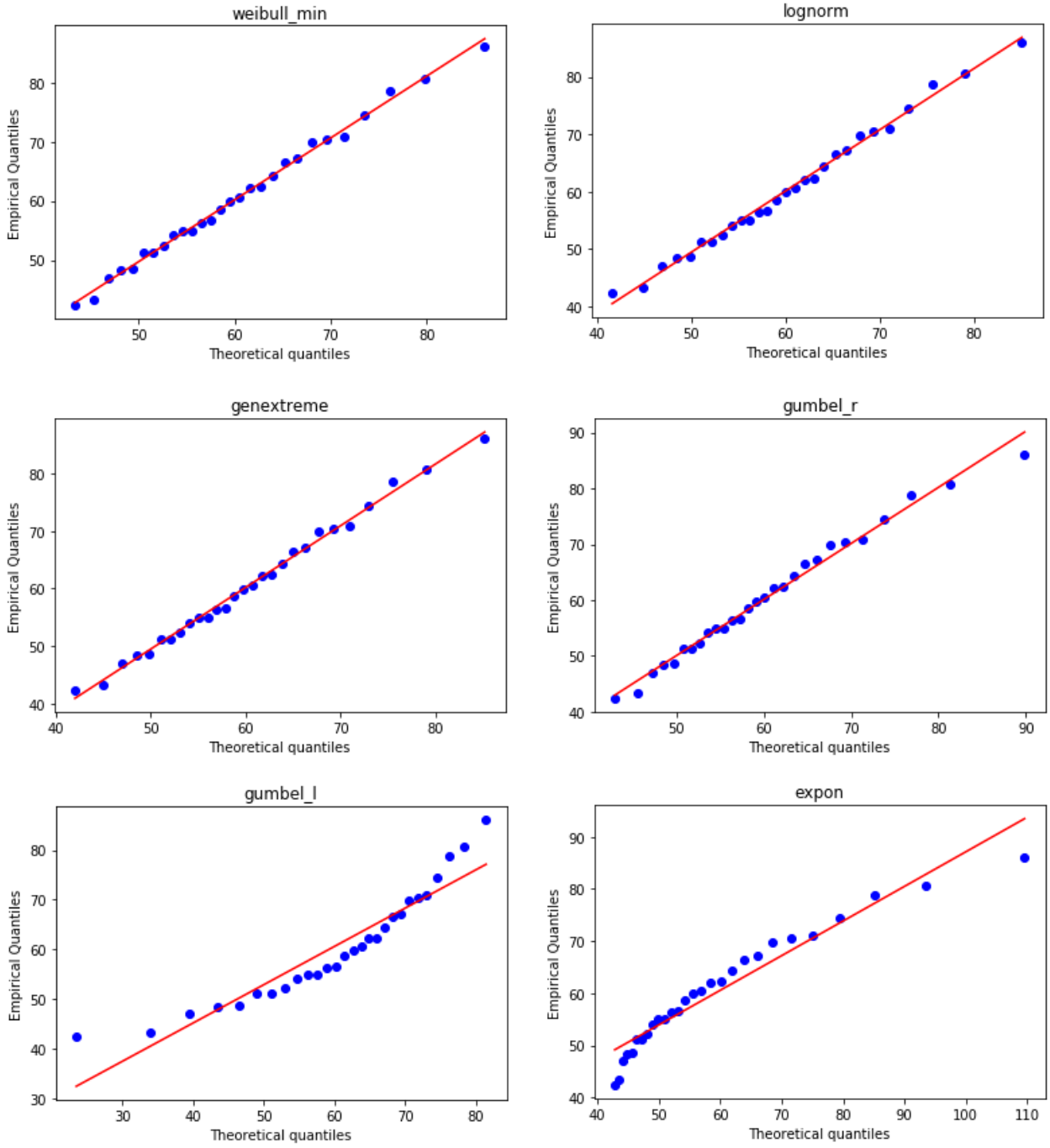

Figure 9.2: QQ-plot of 6 distributions.

D: Storm probability intensity in the PNW

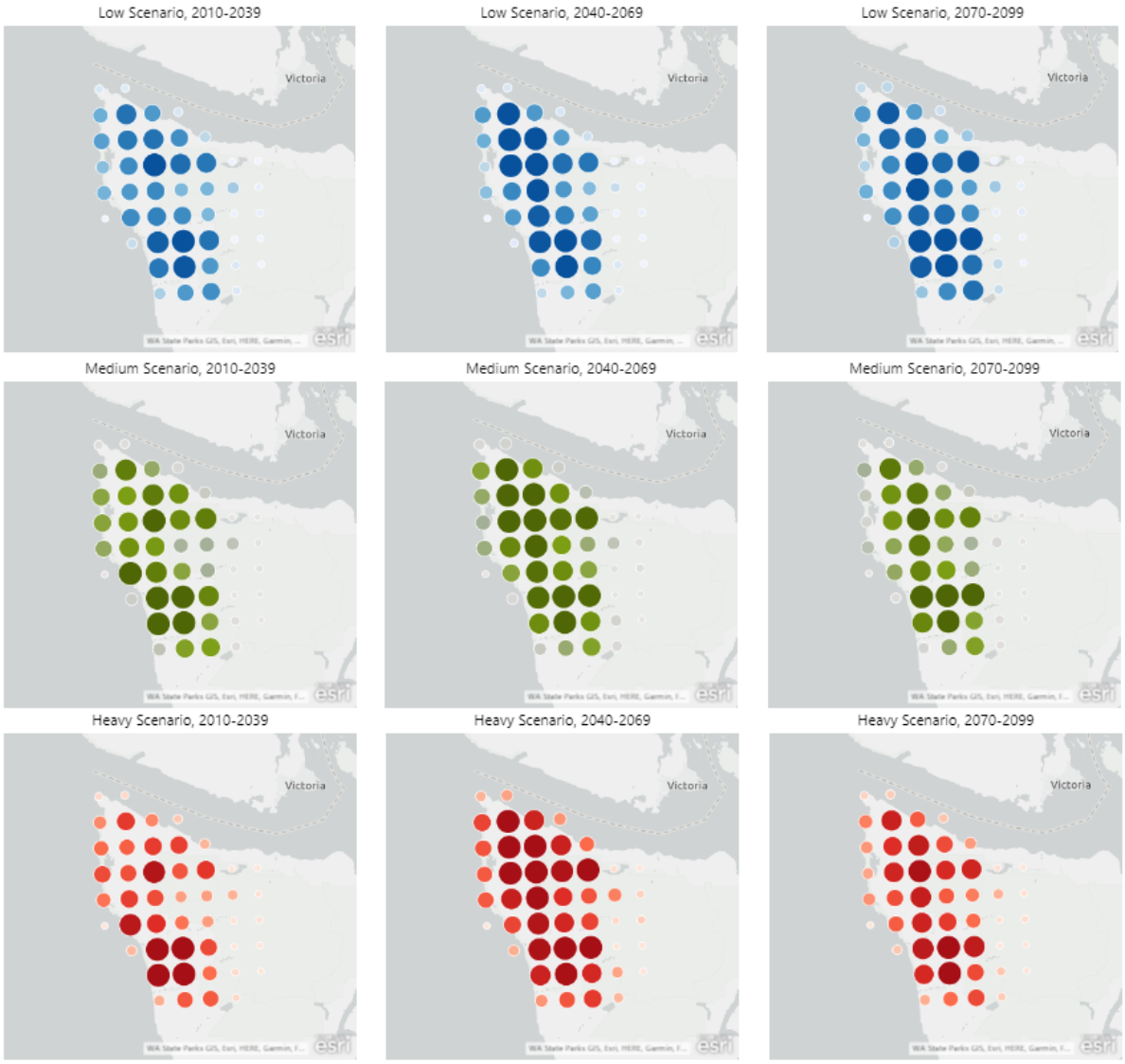

Figure 9.3: Distribution of Storm Probability over tridecade and scenario.

E: Precipitation change intensity in the PNW

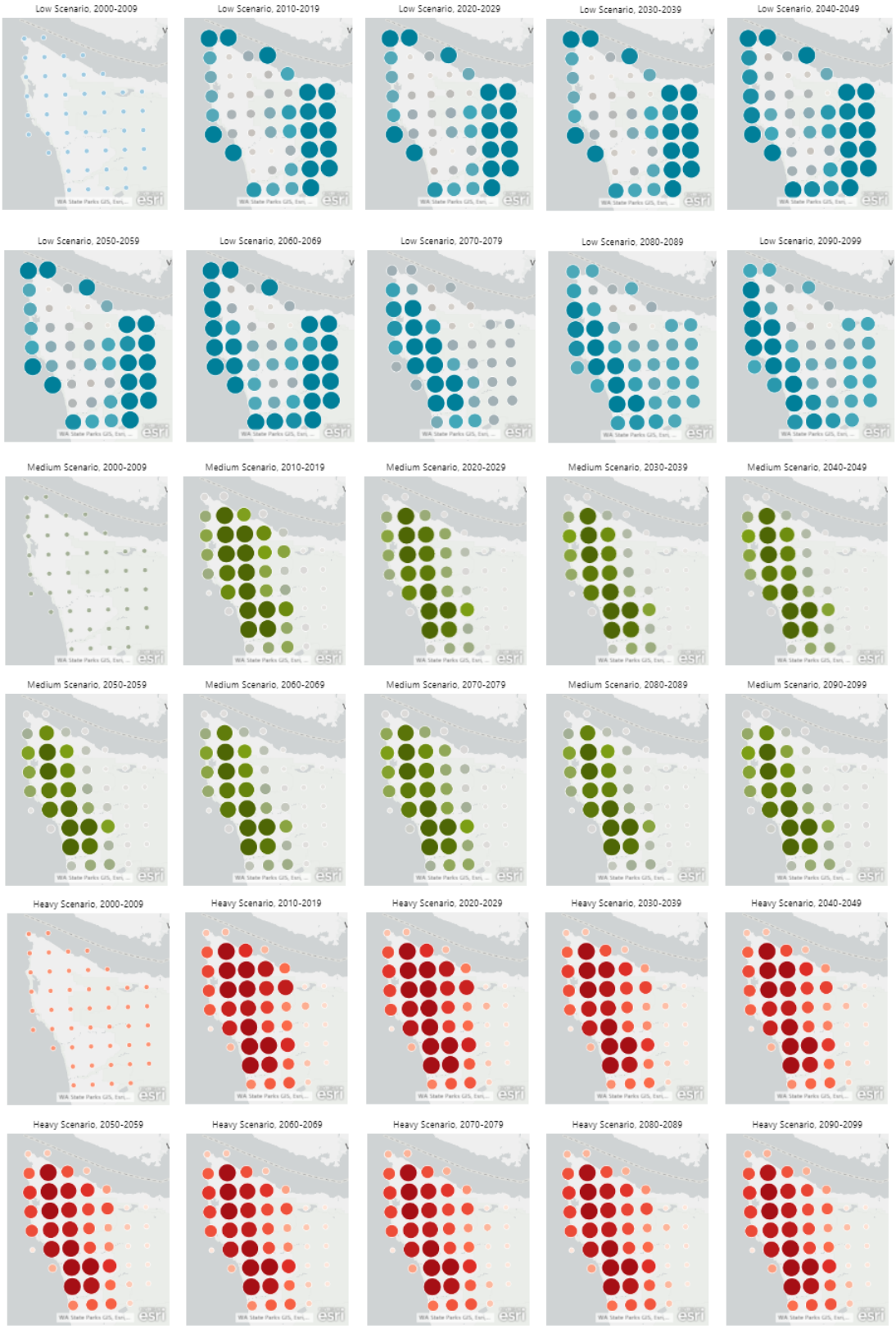

Figure 9.4: Distribution of Precipitation change over decade and scenario.

Bibliography

Alonso-Ayuso, A., Escudero, L. F., Guignard, M., & Weintraub, A. (2018). Risk management for forestry planning under uncertainty in demand and prices. *European Journal of Operational Research*, *267*(3), 1051–1074.

Andalaft, N., Andalaft, P., Guignard, M., Magendzo, A., Wainer, A., & Weintraub, A. (2003). A problem of forest harvesting and road building solved through model strengthening and lagrangean relaxation. *Operations Research*, *51*(4), 613–628.

Bettinger, P., Sessions, J., & Johnson, K. N. (1998). Ensuring the compatibility of aquatic habitat and commodity production goals in eastern oregon with a tabu search procedure. *Forest science*, *44*(1), 96–112.

Bowker, D., Stringer, J., Barton, C., & Fei, S. (2010). Gps and gis analysis of mobile harvesting equipment and sediment delivery to streams during forest harvest operations on steep terrain. In *Proceedings of the 33rd annual meeting of the council on forest engineering: Fueling the future.*

Chinowsky, P., & Arndt, C. (2012). Climate change and roads: A dynamic stressor–response model. *Review of Development Economics*, *16*(3), 448–462.

Diaz, D., Perry, M., Tutak, J., Hodges, R., & Mertens, M. (2015). Potential climate change impacts on management outcomes for western oregon blm forestlands simulated using climate-fvs. ecotrust, portland, or.
doi: 10.13140/RG.2.2.12709.81125.

Elsner, M. M., Cuo, L., Voisin, N., Deems, J. S., Hamlet, A. F., Vano, J. A., ... Lettenmaier, D. P. (2010). Implications of 21st century climate change for the hydrology of washington state. *Climatic Change*, *102*(1-2), 225–260.

Field, C., Barros, V., Dokken, D., Mach, K., MAS-TRANDREA, M., Bilir, T., ... others (2014). Ipcc 2014: Summary for policymakers in climate change 2014: Impacts, adaptation, and vulnerability. part a: Global and sectoral aspects. contribution of working group ii to the fifth assessment report of the intergovernmental panel on climate change. *Contribution of Working Group II to the Fifth Assessment Report of the Intergovernmental Panel on Climate Change*, 1–32.

Flato, G., Marotzke, J., Abiodun, B., Braconnot, P., Chou, S. C., Collins, W., ... others (2014). Evaluation of climate models. In *Climate change 2013: the physical science basis. contribution of working group i to the fifth assessment report of the intergovernmental panel on climate change* (pp. 741–866). Cambridge University Press.

Garcia-Gonzalo, J. (2007). Effects of management on timber production and carbon stocks in a boreal forest ecosystem under changing climate: A model-based approach. *Dissertationes Forestales*, *42*.

Garcia-Gonzalo, J., Pais, C., Bachmatiuk, J., Barreiro, S., & Weintraub, A. (2020). A progressive hedging approach to solve harvest scheduling problem under climate change. *Forests*, *11*(2), 224.

Gillespie, N., Unthank, A., Campbell, L., Anderson, P., Gubernick, R., Weinhold, M., ... others (2014). Flood effects on road–stream crossing infrastructure: economic and ecological benefits of stream simulation designs. *Fisheries*, *39*(2), 62–76.

Halofsky, J. E., Peterson, D. L., O'Halloran, K. A., & Hoffman, C. H. (2011). Adapting to climate change at olympic national forest and olympic national park. *Gen. Tech. Rep. PNW-GTR-844. Portland, OR: US Department of Agriculture, Forest Service, Pacific*

Northwest Research Station. 130 p, *844*.

IPCC. (2018). *What is a gcm?* `http://ipcc-data.org/guidelines/pages/gcm_guide.html`. (Accessed: 2020-23-03)

Johnson, K. N., & Scheurman, H. L. (1977). Techniques for prescribing optimal timber harvest and investment under different objectives—discussion and synthesis. *Forest Science*, *23*(suppl_1), a0001–z0001.

Kirby, M., Wong, P., Hager, W., & Huddleston, M. (1980). Guide to the integrated resource planning model. usda forest service. *Management Sciences Staff, Berkeley, Calif*.

Latta, G., Temesgen, H., & Barrett, T. M. (2009). Mapping and imputing potential productivity of pacific northwest forests using climate variables. *Canadian journal of forest research*, *39*(6), 1197–1207.

Leopold, L. B., & Maddock, T. (1953). *The hydraulic geometry of stream channels and some physiographic implications* (Vol. 252). US Government Printing Office.

Mass, C. (2020). *Amazing murk, very wet on the cascade slopes, and an unusual atmospheric river.* `https://cliffmass.blogspot.com/2020/02/amazing-murk-very-wet-on-cascade-slopes.html?m=1`. (Accessed: 2020-11-03)

Mauger, G., Won, J., Hegewisch, K., Lynch, C., Plazas, R. L., Serra, Y., & Salathé Jr, E. P. (2018). New projections of changing heavy precipitation in king county. *Report prepared for the King County Department of Natural Resources and Parks. Climate Impacts Group, University of Washington, Seattle*.

Nearing, M., Pruski, F., & O'neal, M. (2004). Expected climate change impacts on soil erosion rates: a review. *Journal of soil and water conservation*, *59*(1), 43–50.

Pruski, F., & Nearing, M. (2002). Climate-induced changes in erosion during the 21st century for eight us locations. *Water Resources Research*, *38*(12), 34–1.

Quinteros, M., Alonso-Ayuso, A., Escudero, L. F., Guignard, M., & Weintraub, A. (2011). Forestry management under uncertainty. *Annals of Operations Research*, *190*(1), 17–39.

Raymond, C. L., Peterson, D. L., & Rochefort, R. M. (2014). Climate change vulnerability and adaptation in the north cascades region, washington. *Gen. Tech. Rep. PNW-GTR-892. Portland, OR: US Department of Agriculture, Forest Service, Pacific Northwest Research Station. 279 p.*, *892*.

Riedel, M. S., & Vose, J. M. (2003). Collaborative research and watershed management for optimization of forest road best management practices. In *In: 2003 proceedings of the international conference on ecology and transportation, edited by c. leroy irwin, paul garrett, and kp mcdermott. raleigh, nc: Center for transportation and the environment, north carolina state university. pp. 148-158.*

Ross, K. L., Tóth, S. F., & Jaross, W. S. (2018). Forest harvest scheduling with endogenous road costs. *Interfaces*, *48*(3), 260–270.

Salathé Jr, E. P., Hamlet, A. F., Mass, C. F., Lee, S.-Y., Stumbaugh, M., & Steed, R. (2014). Estimates of twenty-first-century flood risk in the pacific northwest based on regional climate model simulations. *Journal of Hydrometeorology*, *15*(5), 1881–1899.

Sanei Bajgiran, O., Kazemi Zanjani, M., & Nourelfath, M. (2017). Forest harvesting planning under uncertainty: a cardinality-constrained approach. *International Journal of Production Research*, *55*(7), 1914–1929.

Skamarock, W. C., Klemp, J. B., Dudhia, J., Gill, D. O., Barker, D. M., Wang, W., & Powers, J. G. (2005). *A description of the advanced research wrf version 2* (Tech. Rep.). National Center For Atmospheric Research Boulder Co Mesoscale and Microscale ....

Taylor, K. E., Stouffer, R. J., & Meehl, G. A. (2012). An overview of cmip5 and the experiment design. *Bulletin of the American Meteorological Society*, *93*(4), 485–498.

United states v. washington, 2013. case no. cv 70–9213 (w.d. wash.). (2013).

Van Vuuren, D. P., Edmonds, J., Kainuma, M., Riahi, K., Thomson, A., Hibbard, K., ... others (2011). The representative concentration pathways: an overview. *Climatic change*, *109*(1-2), 5.

Veliz, F. B., Watson, J.-P., Weintraub, A., Wets, R. J.-B., & Woodruff, D. L. (2015). Stochastic optimization models in forest planning: a progressive hedging solution approach. *Annals of Operations Research*, *232*(1), 259–274.

Warner, M. D., Mass, C. F., & Salathé Jr, E. P. (2015). Changes in winter atmospheric rivers along the north american west coast in cmip5 climate models. *Journal of Hydrometeorology*, *16*(1), 118–128.

Weintraub, A., & Navon, D. (1976). A forest management planning model integrating silvicultural and transportation activities. *Management Science*, *22*(12), 1299–1309.

Wilhere, G. F., Atha, J. B., Quinn, T., Tohver, I., & Helbrecht, L. (2017). Incorporating climate change into culvert design in washington state, usa. *Ecological Engineering*, *104*, 67–79.